IDO-17203
February 1967

5

RADIOLOGICAL ASPECTS OF THE SNAPTRAN-2 DESTRUCTIVE TEST

By
O. L. Cordes
D. F. Bunch (AEC)
J. R. Fielding
J. K. Warkentin

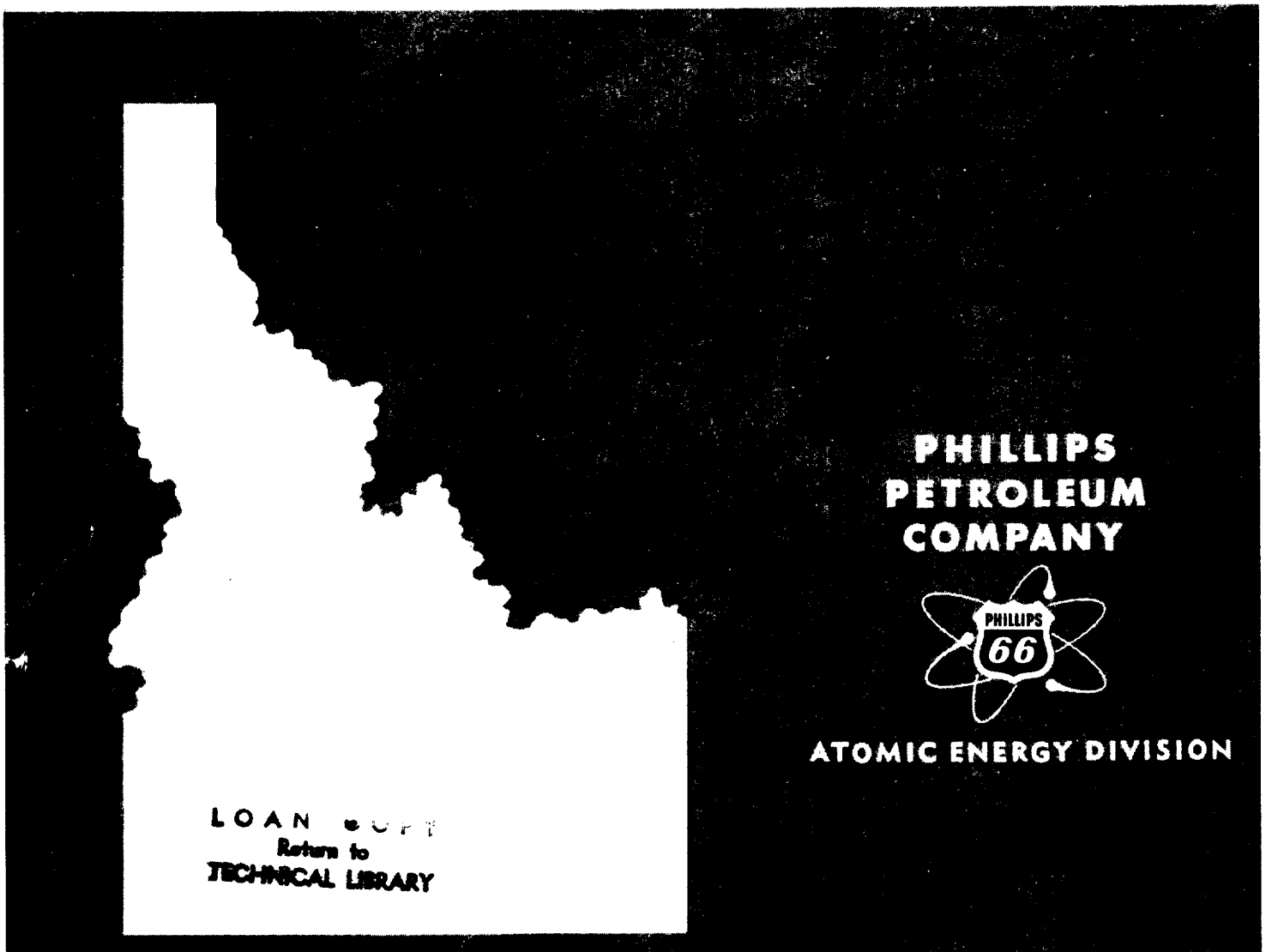

Printed in the United States of America
Available from
Clearinghouse for Federal Scientific and Technical Information
National Bureau of Standards, U. S. Department of Commerce
Springfield, Virginia 22151
Price: Printed Copy $3.00; Microfiche $0.65

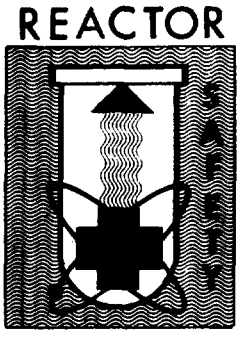

IDO-17203
AEC Research and Development Report
Reactor Technology
TID-4500
Issued: February 1967

RADIOLOGICAL ASPECTS OF THE SNAPTRAN-2 DESTRUCTIVE TEST

BY

O. L. Cordes
D. F. Bunch (AEC)
J. R. Fielding
J. K. Warkentin

PHILLIPS
PETROLEUM
COMPANY

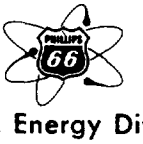

Atomic Energy Division
Contract AT(10-1)-205
Idaho Operations Office
U. S. ATOMIC ENERGY COMMISSION

ACKNOWLEDGEMENTS

The authors wish to acknowledge R. A. Jensen, P. E. Ruhter, A. L. Smith, and D. R. Wenzel for their aid in the collection and reduction of data for this report. Valuable assistance and suggestions in the report content and form were also given by F. L. Bentzen and G. A. Dinneen.

ABSTRACT

Radiological information obtained from monitoring a planned destructive excursion of a modified SNAP 10A/2 reactor is described in this report along with the sampling and analytical techniques used to obtain the information. An analysis of the data is included which indicates that only 21 percent of the fission products were released, that the radiation hazards were low, and that the beryllium from the reactor drums and reflectors did not produce a health hazard.

CONTENTS

FIGURES

TABLES

I. INTRODUCTION

As a continuation of the safety program inaugurated by the United States Atomic Energy Commission to assess the nuclear and radiation safety problems of small space reactors, a second SNAP 10A/2 reactor was intentionally destroyed in a Reactor Safety Test Program conducted by Phillips Petroleum Company at the National Reactor Testing Station in Idaho.

As part of a series of safety tests, designated the SNAPTRAN Program, test versions of two SNAP 10A/2 reactors were subjected to severe reactivity insertions which resulted in their complete destruction. The first of these two tests, SNAPTRAN-3, was designed to provide information on the radiological consequences of the accidental immersion of a SNAP 10A/2 reactor in water or wet earth such as could occur during assembly, transport, or a launch abort. The second of these tests, SNAPTRAN-2, was designed to provide information on the dynamic response, the fuel behavior, and the inherent shutdown mechanisms of these reactors in an open air environment.

The SNAPTRAN-3 destructive test was completed in April 1964, and the radiological results from that test are reported in IDO-17083[1]. The following report describes the radiological aspects of the SNAPTRAN-2 destructive test which was conducted on January 11, 1966. Included in this report are descriptions of the reactor, the radiological monitoring program, test meteorological requirements, and a presentation and analysis of the radiological results determined from the SNAPTRAN-2 test.

II. REACTOR TEST PACKAGE DESCRIPTION

A typical cross section of a SNAP 10A/2 reactor is shown in Figure 1. Thirty-seven fuel rods, held by upper and lower grid plates, were arranged in a close-packaged hexagonal array to form the core of the reactor. Six beryllium filler pieces around the hexagonal core adapted it to a cylindrical stainless steel vessel approximately 23 cm in diameter and 31 cm in height. The fuel-moderator for this reactor was an alloy of zirconium hydride and 10 weight percent of highly enriched (93 percent) uranium. With this configuration, the SNAPTRAN-2 core contained 4.75 kg of U-235 and 464 gram moles of hydrogen.

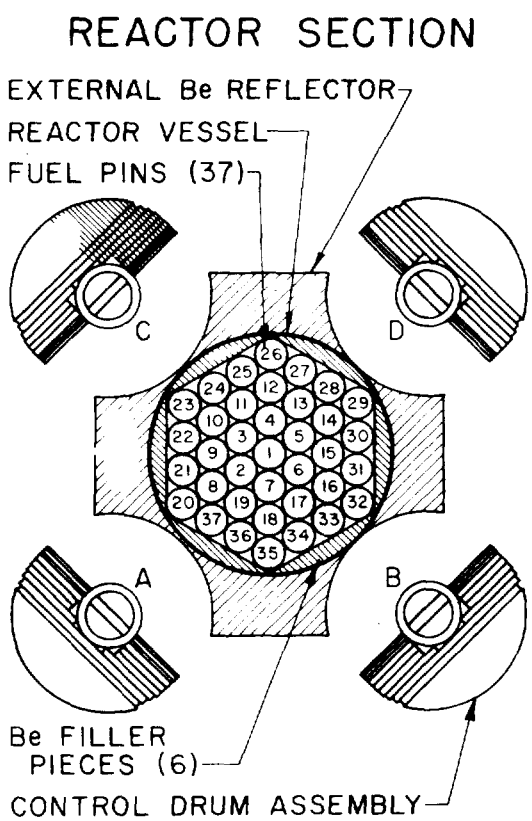

Fig. 1 Reactor cross section.

Although the normal flight system reactors contain NaK for a coolant, the SNAPTRAN-2 test was conducted without NaK. The absence of the NaK had little nuclear reactivity effect and allowed high speed photographs to be taken through the core interstices to observe the development of radial core growth and local mechanical effects due to hydrogen release.

The reactor was controlled by the four beryllium drums spaced 90 degrees apart in round slots in the fixed beryllium reflector. These drums had the capability of being rapidly rotated thus providing a mechanism to add or withdraw reactivity. The destructive test was initiated by rotating and stopping the drums in their most reactive position.

The SNAPTRAN-2 reactor test package was mounted on a special four-rail flatcar (Figure 2) to facilitate transportation between the test area and the examination and assembly areas. The reactor test package was held in position on the flatcar by a structural framework. A ramp was also constructed from ground level to the reactor test package to provide a route for a remote-controlled track-driven manipulator (mobot) to reach the reactor in the event of an equipment malfunction.

Reactor operation and initiation of the destructive test were accomplished from an underground, shielded control building adjacent to the reactor test pad. A shielded roadway tunnel gave access to the underground area. The test cell building, also mounted on railroad wheels and steel tracks, was pulled over from the test pad prior to initiation of the test, leaving the reactor in an essentially open area.

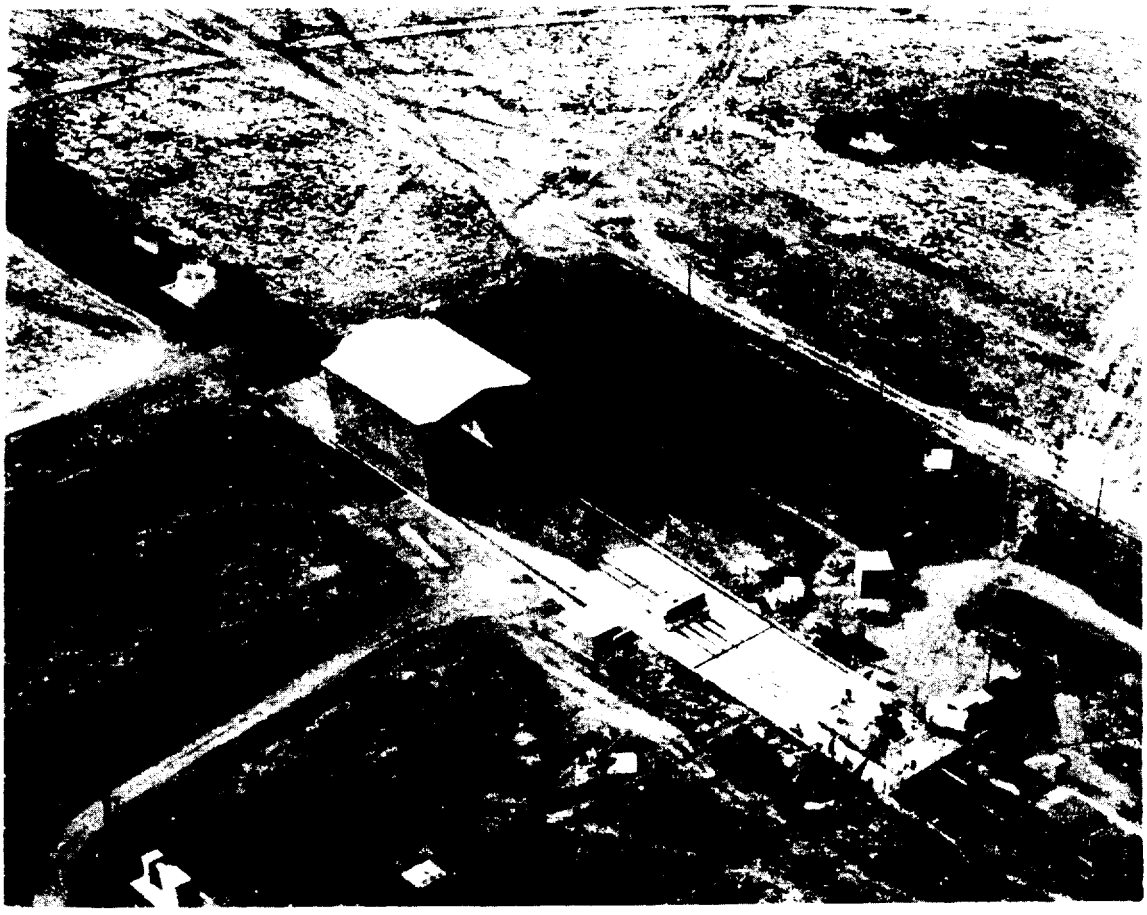

Fig. 2 Test area and the reactor assembly.

III. RADIOLOGICAL MONITORING PROGRAM

In order to determine the radiological consequences of the SNAPTRAN-2 test, a radiological monitoring network was set up around the reactor test pad. This monitoring network was similar to that used for the earlier SNAPTRAN-3 destructive test[1] with a heavy concentration of sampling equipment located on arcs in the prevailing downwind direction.

The monitoring program was a joint effort of the Health and Safety Branch of Phillips Petroleum Company and the Health and Safety Division of AEC Idaho Operations Office. Phillips Petroleum Company was responsible for monitoring out to a distance of 1600 meters and the ID Health and Safety Division was responsible for distances beyond 1600 meters. The ID Health and Safety Division was also responsible for aerial tracking and sampling of the radioactive cloud. In addition to the radiological monitoring effort, information on test weather conditions and cloud trajectories was provided by the Air Resources Field Research Office (ARFRO) of the Institute for Atmospheric Sciences.

The monitoring network included a radiological monitoring grid (Figures 3, 4, 5, 6) which was set up as a series of concentric arcs with the reactor test pad at the center. A heavy concentration of sampling equipment was placed in a 60 degree sector, orientated with its center on the anticipated "cloud" trajectory 30 degrees east of true north. In addition to the instrumentation on the grid, samplers were located in various areas near the off-site populated regions, in the surrounding towns, and on the test pad adjacent to the reactor.

The grid samplers were positioned on steel posts approximately one meter above the ground to obtain samples from the radioactive cloud as it diffused downwind. At three locations, a series of samplers was located at various elevations above the terrain to gain information on the initial height of the cloud and to sample the vertical distribution of the radioactive material in the cloud. These samplers were at 46, 18, and 15 meters above the ground.

The types of samplers used in the monitoring network consisted mainly of high-volume air samplers, fission gas detectors, fallout plates, radiation dosimeters, and particle size samplers.

The high-volume air samplers were equipped with a high-efficiency particulate filter (Microsorban)[2] and a charcoal bed (BM 2306)[3] in series. The high-efficiency particulate filter collected the radioactive particulate material while the charcoal bed collected the iodine and a portion of the noble gases.

The fission-gas detectors (Figure 7) were designed to obtain a sample of the noble gases from the cloud as it moved past the sampling point. Air containing the radioactive noble gases was drawn into an airtight balloon through a particulate filter and stored in the balloon while the gases decayed into their particulate daughters. After a prescribed length of time, the balloon was deflated through a second high-efficiency filter. The amount of daughter formed during the decay interval was determined by gamma-ray counting of both the filter and the deflated balloon. The concentration of the parent gas was then calculated from the amount of daughter activity collected.

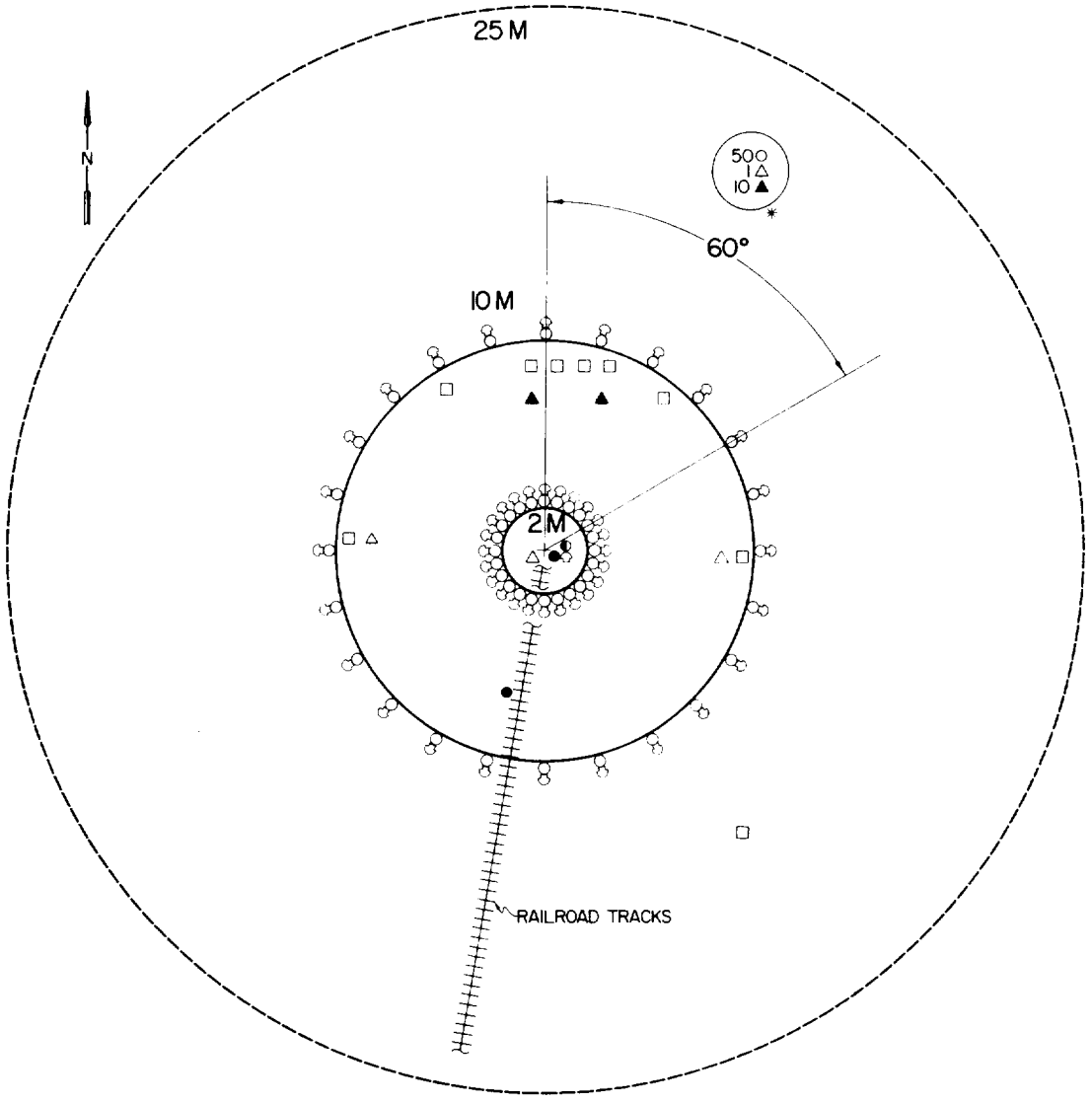

○ FILM BADGES, FALLOUT PLATES AND POCKET DOSIMETERS
✳ RADIOLOGICAL SURVEILLANCE TOWER
○ POLYMERIZATION, CHEMICAL AND GLASS DOSIMETERS
▲ HIGH-VOLUME AIR SAMPLERS
△ REMOTE AREA MONITOR
□ FILM BADGE DROPS
● NUCLEAR ACCIDENT DOSIMETERS

Fig. 3 SNAPTRAN radiological grid, 2- and 10-meter arcs.

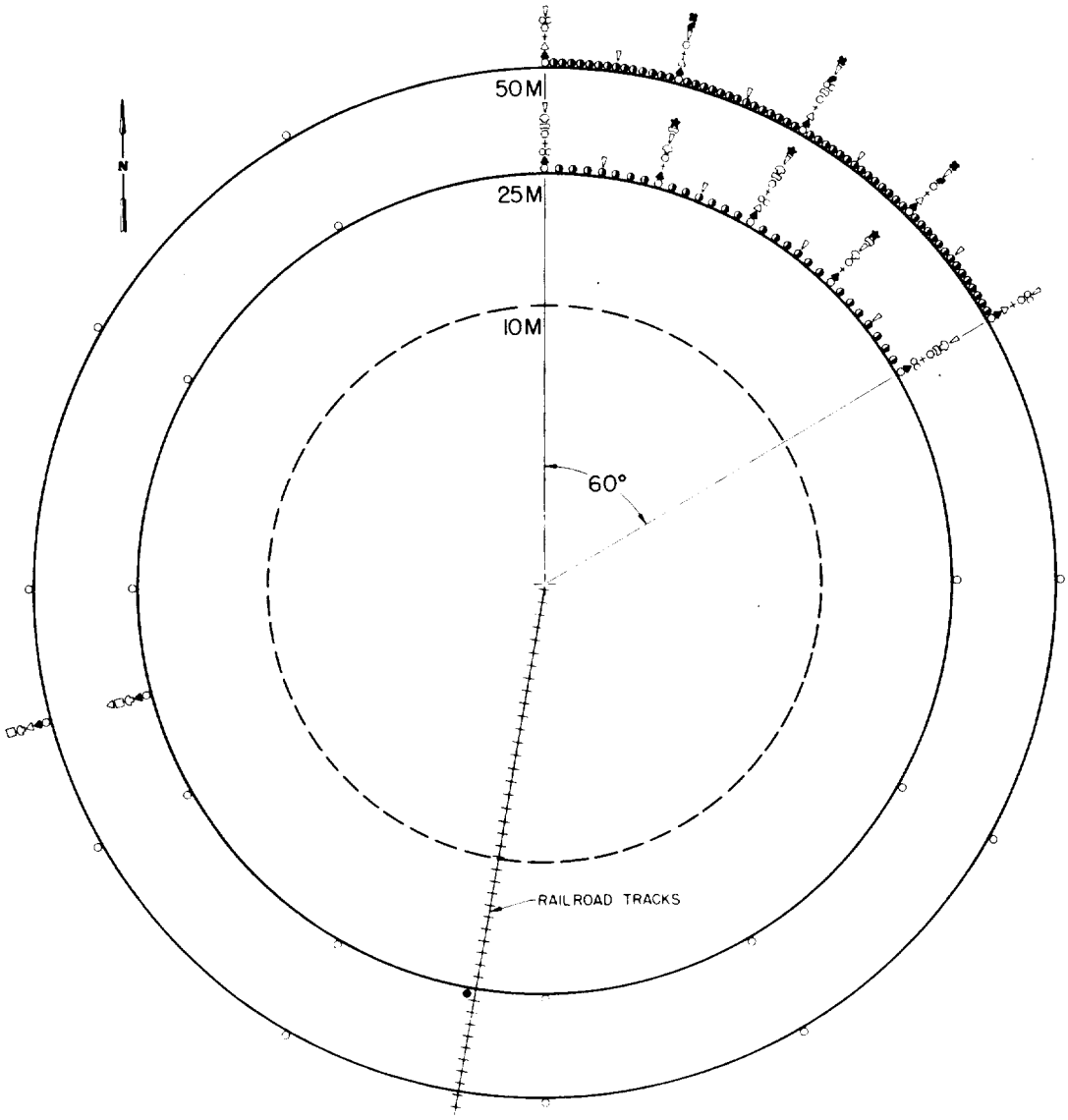

Fig. 4 SNAPTRAN radiological grid, 25- and 50-meter arcs.

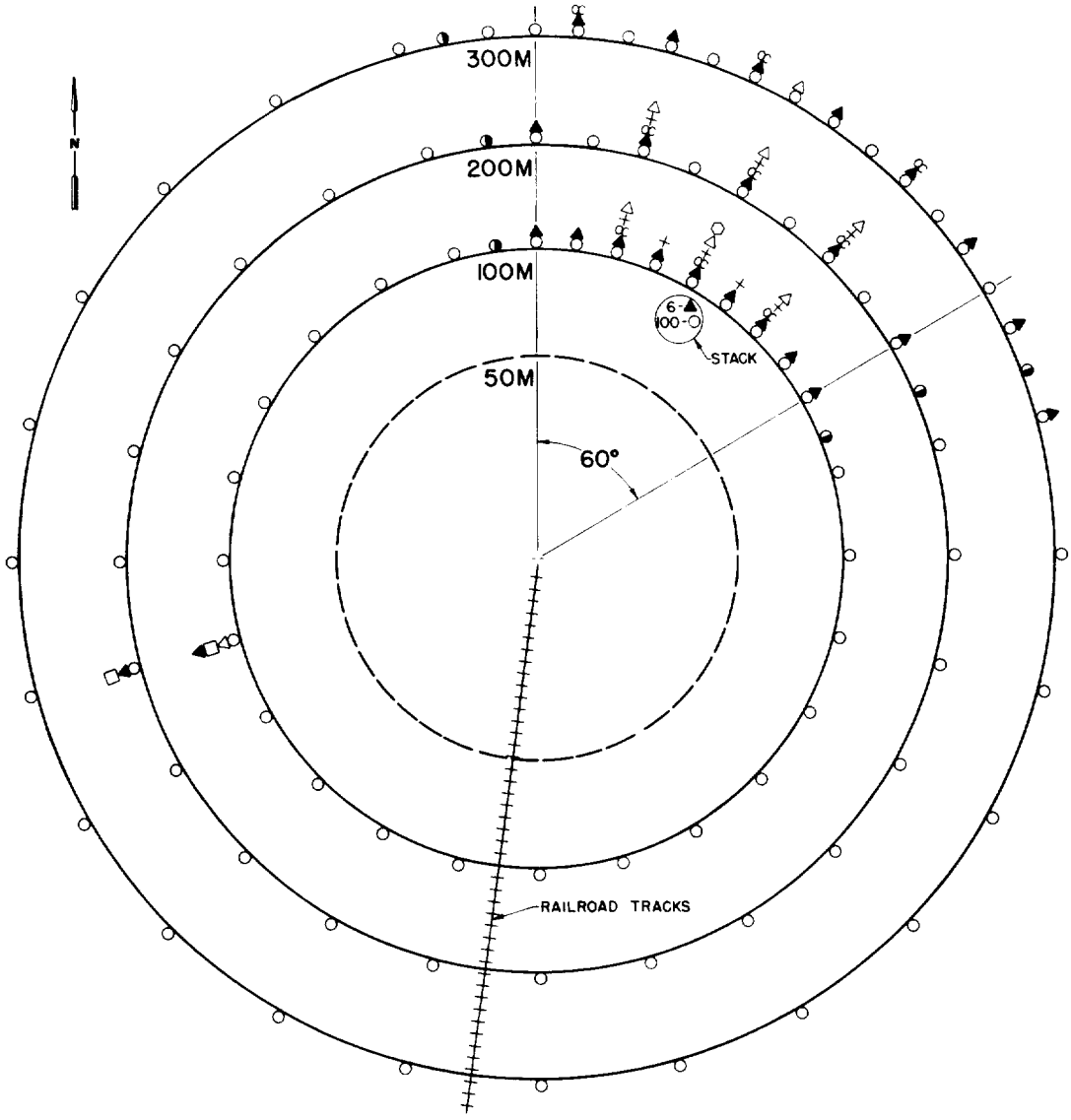

Fig. 5 SNAPTRAN radiological grid, 100-, 200-, and 300-meter arcs.

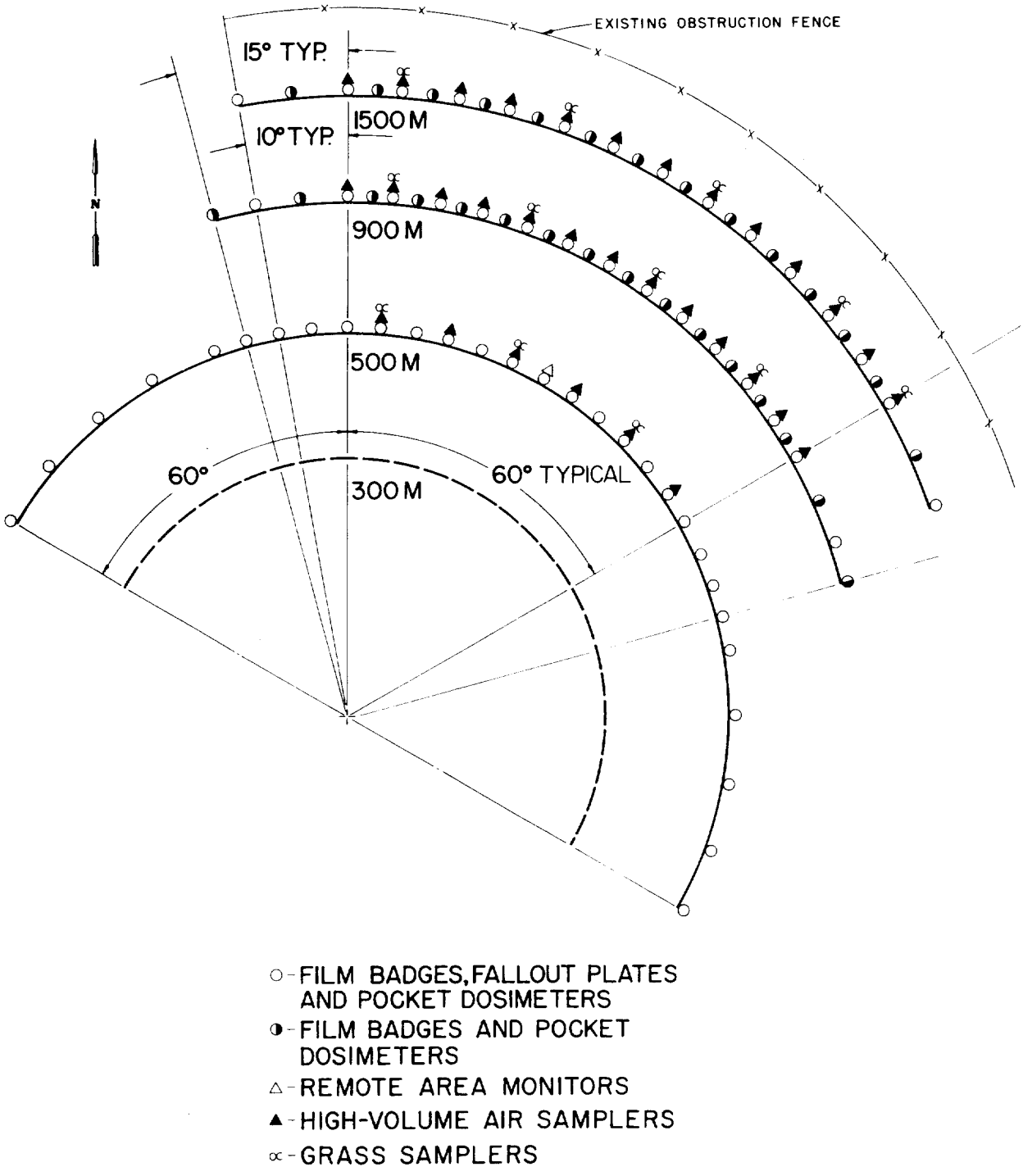

Fig. 6 SNAPTRAN radiological grid, 500-, 900-, and 1500-meter arcs.

The film dosimeters were used to measure the direct radiation effects from the reactor and from the radioactive cloud. The dosimeters contained duPont film packets in special NRTS film badge dosimeter holders which have graded metal filters to allow a determination of beta exposure as well as gamma-ray exposure. The film dosimeter is capable of measuring doses in the range 20 mR to 600 R. In positions where radiation doses were expected to be higher than the 600 R maximum range of the film dosimeter, chemical and thermoluminescent dosimeters (TLD's) were used. The range covered by these dosimeters was from 20 mR to 10^5 R.

Neutron dosimetry to obtain total integrated neutron exposures was performed using the ORNL-Hurst type nuclear accident dosimeters[6] (NAD's), thermoluminescent dosimeters, and gold activation foils. These dosimeters were capable of measuring neutron fluxes in both the thermal and fast energy regions.

The aircraft used for radiological monitoring and surveillance during the test carried high-volume air samplers and direct-radiation dose-rate meters to measure the cloud dose rates, cloud dimensions, and cloud particulate and iodine concentrations.

IV. METEOROLOGICAL PARAMETERS

In order to minimize the radiological hazards from the destruction of the reactor and to ensure that the radioactive cloud from the test would pass over the heavily instrumented section of the monitoring grid, a specific set of weather conditions for initiation of the test was agreed upon by Phillips Petroleum Company, Idaho Operations Office, USAEC, and ARFRO of the Institute of Atmospheric Sciences. These weather conditions were as follows:

(1) Wind directions from the S-SW (180 degrees - 240 degrees) to ensure that the cloud pass over the heavily instrumented section of the grid.

(2) Wind speed between 3 and 18 meters per second. The upper limit of 18 mps was established to assure safe aerial monitoring, and the lower range restriction was added to obtain a predictable stable wind which was not subject to rapid directional changes.

(3) No imminent precipitation in the vicinity of the test. This restriction avoided the possibility of "washout" of radioactive material before the cloud could be sampled.

(4) Vertical temperature profile of neutral to light lapse conditions required to prevail for 30 minutes following the test to assure adequate diffusion of radioactive debris.

To prepare for the test, ARFRO conducted a careful weather analysis of pressure systems and trends for several weeks prior to the test. On January 8, 1965, ARFRO predicted that favorable weather conditions would occur on several days beginning January 11, 1966, and test preparation was initiated.

V. TEST OPERATION

On January 11, 1966, after early morning preparations both on the radiological grid and at the underground control center, the reactor test pad and downwind areas were cleared of personnel. Countdown procedures for the destructive test were initiated and continued on schedule until five minutes prior to initiation of the test. At this point everything was held in readiness waiting for the desired weather conditions. As forecasted, a frontal system passed over the area at about 0900 bringing with it the possibility of S-SW wind and lapse conditions. At 0940 the wind velocity reached 5 mps, and the vertical temperature profile indicated a neutral to light lapse condition. Test countdown was resumed and proceeded to the successful initiation of the test at 0951 MST on January 11, 1966.

Complete disruption of the reactor was evident through visual observation from the mile exclusion fence. Pieces of burning fuel and reactor debris were observed to be scattered over the test pad and surrounding area.

The sequence of the core disassembly is shown in Figures 8 through 15. Gross core destruction took place as can be seen by the wide-spread pieces of burning fuel. The visible smoke-filled cloud arose immediately following the test. This cloud reached a height of 30 meters after it had traveled 20 meters downwind and leveled off at about 50 meters high by the time it had reached 100 meters downwind. It was assumed that the airborne radioactive debris released from the reactor behaved in the same manner as the visible cloud.

The instrumented aircraft began monitoring the cloud radiation immediately and followed the cloud on a downwind course determined from visual observations of a balloon released by ARFRO. The plane, while flying at 150 meters above the terrain, intercepted the cloud 300 meters downwind from the reactor. At this time a detector aboard the craft recorded a dose rate of 500 mR/hr. At this corresponding downwind distance a ground level dose rate of 2.7 R/hr was recorded by a remote area detector. The aircraft and ground level telemetering stations continued to monitor the cloud as it moved beyond the site boundary (10 kilometers downwind). The cloud was followed out to a distance of about 30 kilometers at which point radiation levels were not distinguishable from background radiation, which is about 0.2 mR/hr.

Closed-circuit TV scanning devices on the test pad allowed immediate evaluation of the state of the reactor and also confirmed the early information which indicated that the reactor had been completely disassembled. The complete disruption of the reactor removed the possibility of a secondary criticality, and the test area was opened for reentry teams to examine the reactor remains and recover samples. A few pieces of fuel rods were observed as far away as 200 meters from the reactor with a greater concentration of dispersed fuel and beryllium pieces near the test pad. Radiation dose rates were low at this time (1-1/2 hours after the test). Dose rates were generally at normal background levels 100 meters from the test pad increasing to 25 R/hr at 10 meters from the test pad. The test pad and the immediate surrounding area were highly contaminated with dispersed reactor fuel and contaminated debris.

Sample recovery teams began retrieving samples from the radiological grid and from around the reactor test pad about two hours after the test. Radio-equipped vehicles carrying air-monitoring and direct-radiation measuring instruments were used to provide assessment and warning of hazards to personnel. All grid samples were collected, sealed in plastic bags, and sent to the analytical groups for analysis by 1800 hours.

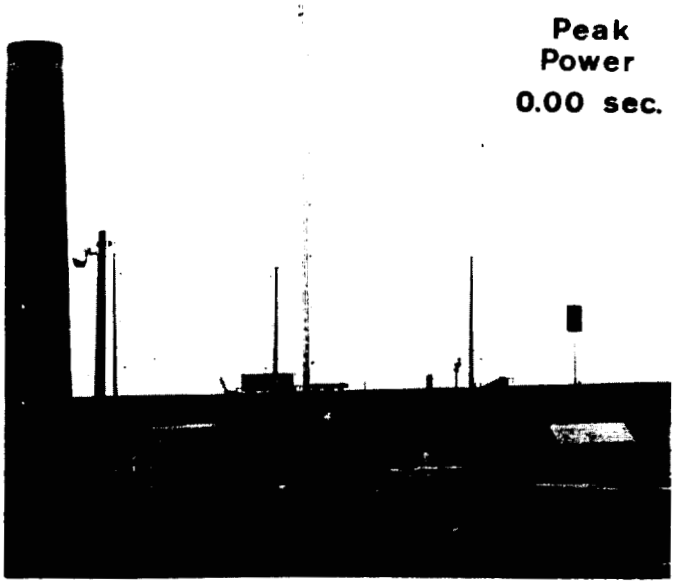

Fig. 8 Snaptran-2 Core Disassembly Sequence

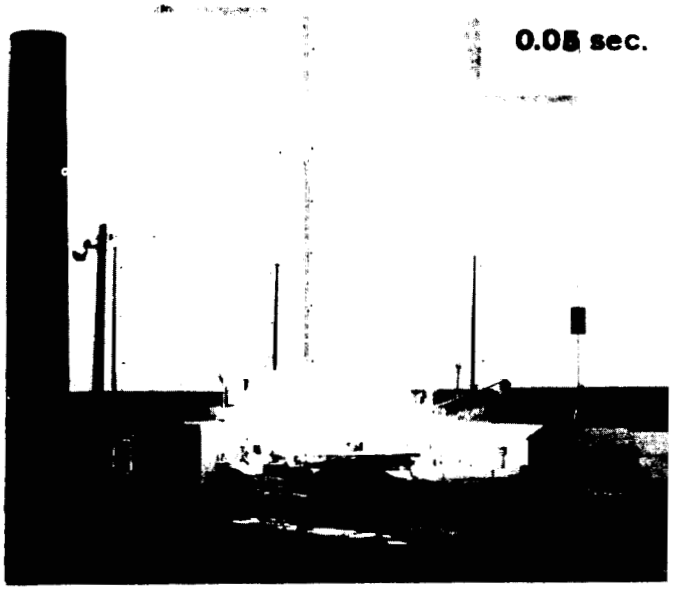

Fig. 9 Snaptran-2 Core Disassembly Sequence

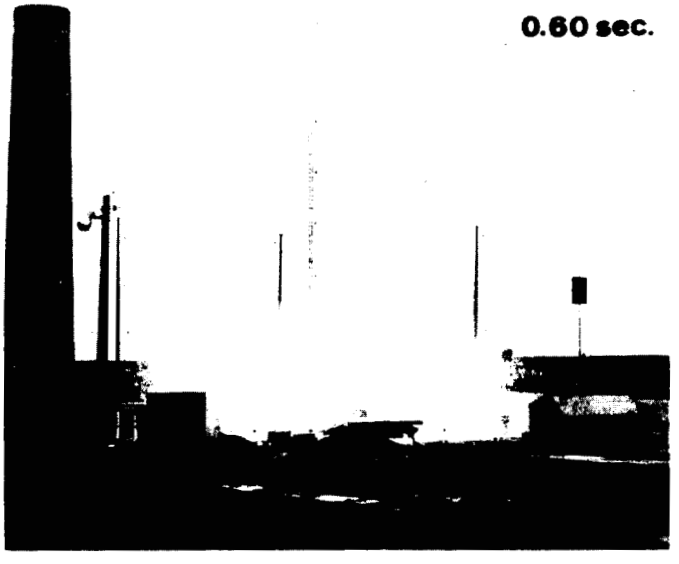

Fig. 10 Snaptran-2 Core Disassembly Sequence

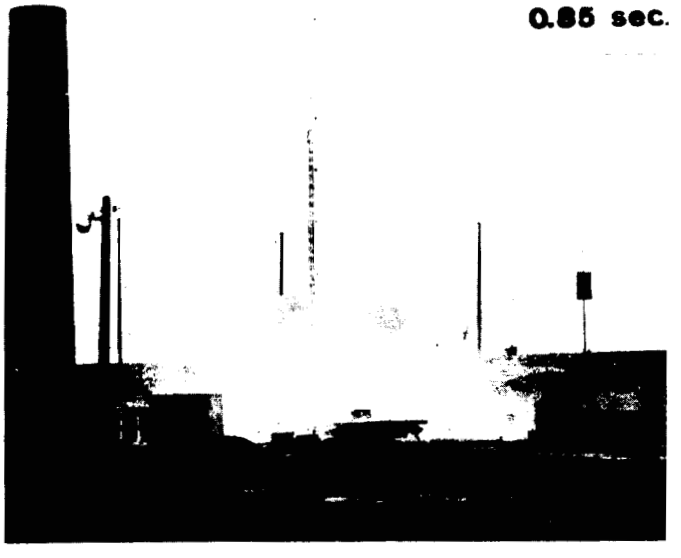

Fig. 11 Snaptran-2 Core Disassembly Sequence

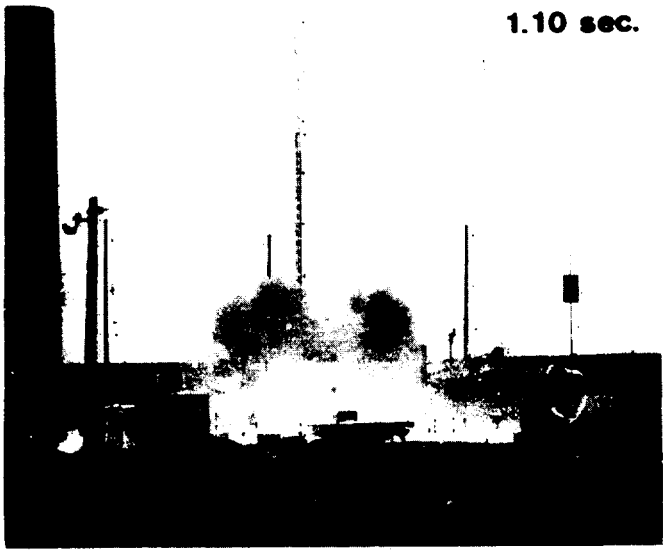

Fig. 12 Snaptran-2 Core Disassembly Sequence

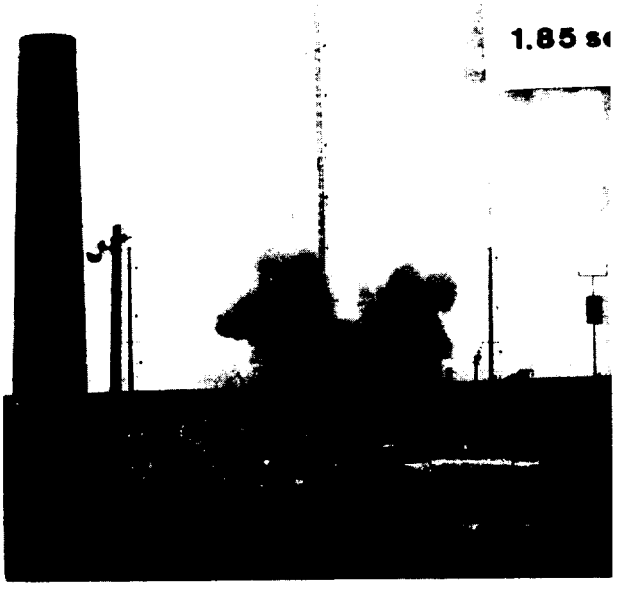

Fig. 13 Snaptran-2 Core Disassembly Sequ

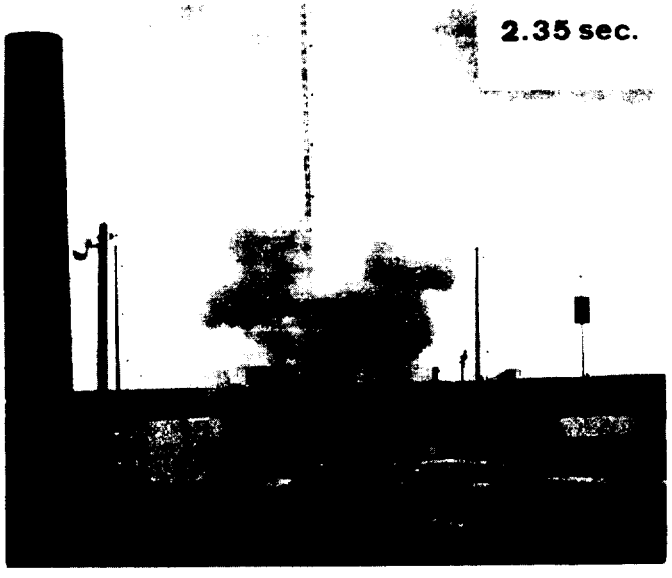

Fig. 14 Snaptran-2 Core Disassembly Sequence

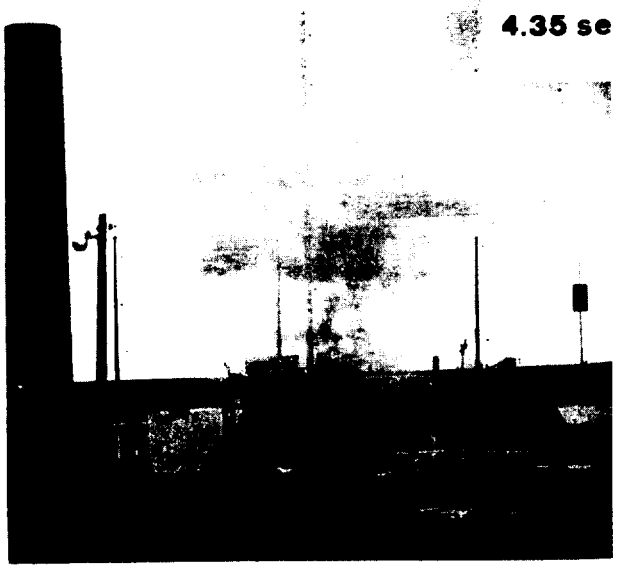

Fig. 15 Snaptran-2 Core Disassembly Sequ

VI. REACTOR PHYSICS DATA[7]

The disassembly of the reactor resulted from the rapid stepwise addition of essentially all the available excess reactivity. The reactivity insertion was accomplished in two steps. The first step-reactivity addition brought the reactor from a subcritical state to about 40 cents supercritical. One-half second later, the second step-reactivity addition of 4.7 dollars was introduced. The final step addition was complete in 12 msec, 8 msec prior to the time of peak power and 4 to 6 msec prior to the onset of sensible heat, which produced negative reactivity feedback. A 200 μmsec reactor period resulted from the reactivity addition. The period persisted until approximately 0.75 msec prior to reaching a peak power of 74,000 MW. Immediately following peak power, the effects of radial core expansion reduced the reactivity state of the reactor to its ultimate shutdown state. During the 1 msec prior to and the 0.5 msec following peak power, a total of 54 MW-sec of nuclear energy was released.

VII. RADIOLOGICAL RESULTS

1. DOSE RATE MEASUREMENTS

The direct-radiation dose rates resulting from the destructive excursion, the radioactive cloud, and the decay of the fission product debris in the reactor area were monitored and recorded by 21 remote radiation detectors located on the radiological grid. During the first five seconds following the test, the remote detectors within a radius of 20 meters from the reactor were driven off scale at 1000 R/hr. At this same time, recorders from detectors located at a distance of 25 meters upwind recorded a maximum dose rate of 800 R/hr. However, the actual peak dose rate from the reactor transient was higher than recorded by these remote detectors because the recording systems on these detectors were unable to follow the rapid rise and decay of the transient dose rate during this period. Some of the remote detectors were located in an upwind unshielded position to measure the dose rates from the reactor and debris while the downwind detectors measured both the dose rates due to the reactor and debris and the radioactive cloud. The gamma dose rates at these three upwind locations are shown as a function of time in Table I.

TABLE I

GAMMA DOSE RATES (R/hr) AS A FUNCTION OF TIME AND DISTANCE

Grid Location	Distance (meters)	Minutes Following Test						
		2	5	10	15	20	25	30
A-40	25	330	98	49	33	25	20	17
B-70	50	70	23	10	6.2	4.6	3.7	3.2
C-29	100	4	1.4	0.6	0.39	0.28	0.21	0.15

Figure 16 is a plot of the gamma dose rate as a function of time as monitored on the 100 meter arc. Also included in the figure is a curve calculated from the empirical expression $R = kt^{-1.2}$ where R equals rate of gamma emission, k equals constant, and t equals time in seconds. The calculated dose rate approximates the measured dose rate during this time interval.

A close-in measurement in the reactor area was obtained from a detector located at six meters from the reactor. The dose rates at various times following the test are shown in Table II.

The downwind dose rates, which were primarily due to the debris-laden cloud as it passed over the grid, are shown in Figure 17. The direct radiation from the reactor remnants made only a small contribution to the total downwind dose rates compared with the radiation from the cloud. The peak cloud dose rate measurements obtained at various distances are listed in Table III.

The prompt gamma dose rate from the excursion was measured by detectors with extremely short response times and was recorded on high-speed magnetic

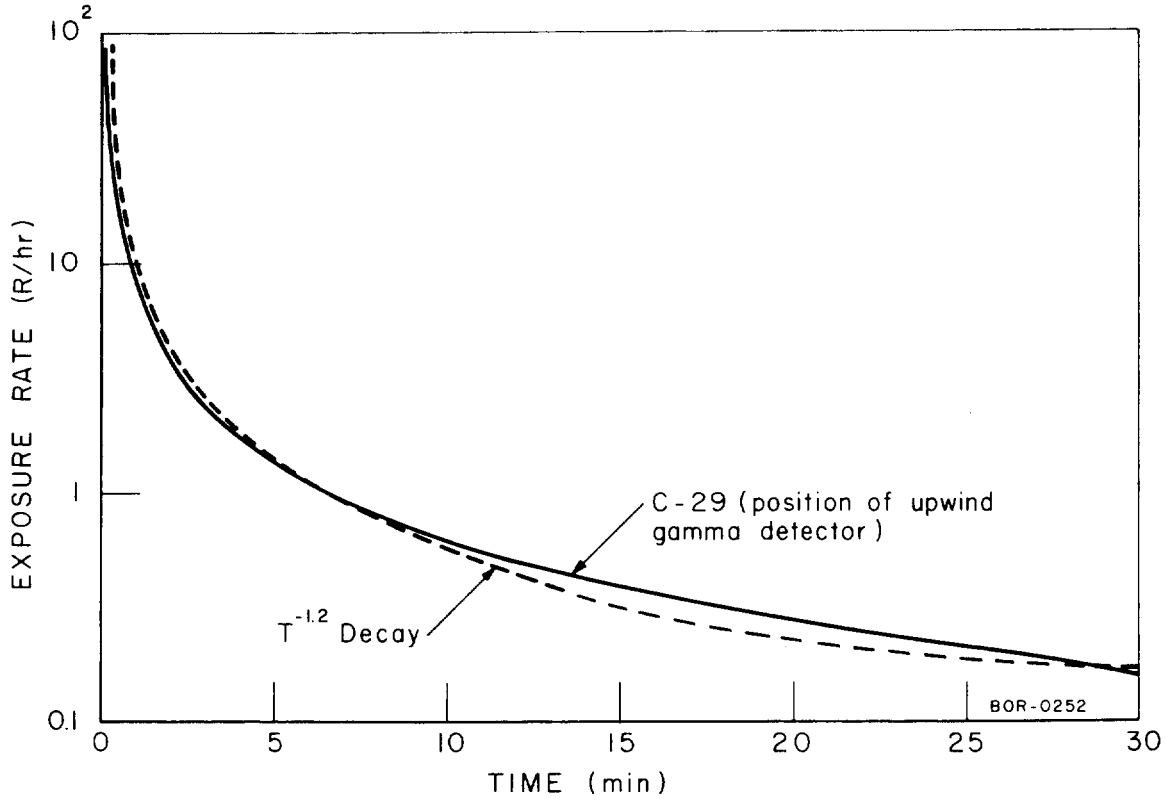

Fig. 16 Decay of fission products (measured versus theoretical).

TABLE II

GAMMA DOSE RATE AS A FUNCTION OF TIME AT SIX METERS

Time After Test (hrs)	Dose Rate (R/hr)
2-1/4	18
4-3/4	9
6-1/4	6
24	0.8
48	0.2

TABLE III

GROUND LEVEL CLOUD DOSE RATES

Distance (meters)	Maximum Dose Rate (mR/hr)
4,000	20
8,400	1
16,000	0.2

tape. A graph of the prompt gamma dose rate versus time for a detector positioned 2.2 meters from the reactor is shown in Figure 18. The peak dose rate recorded by the detector at this location was 1.7×10^{10} R/hr.

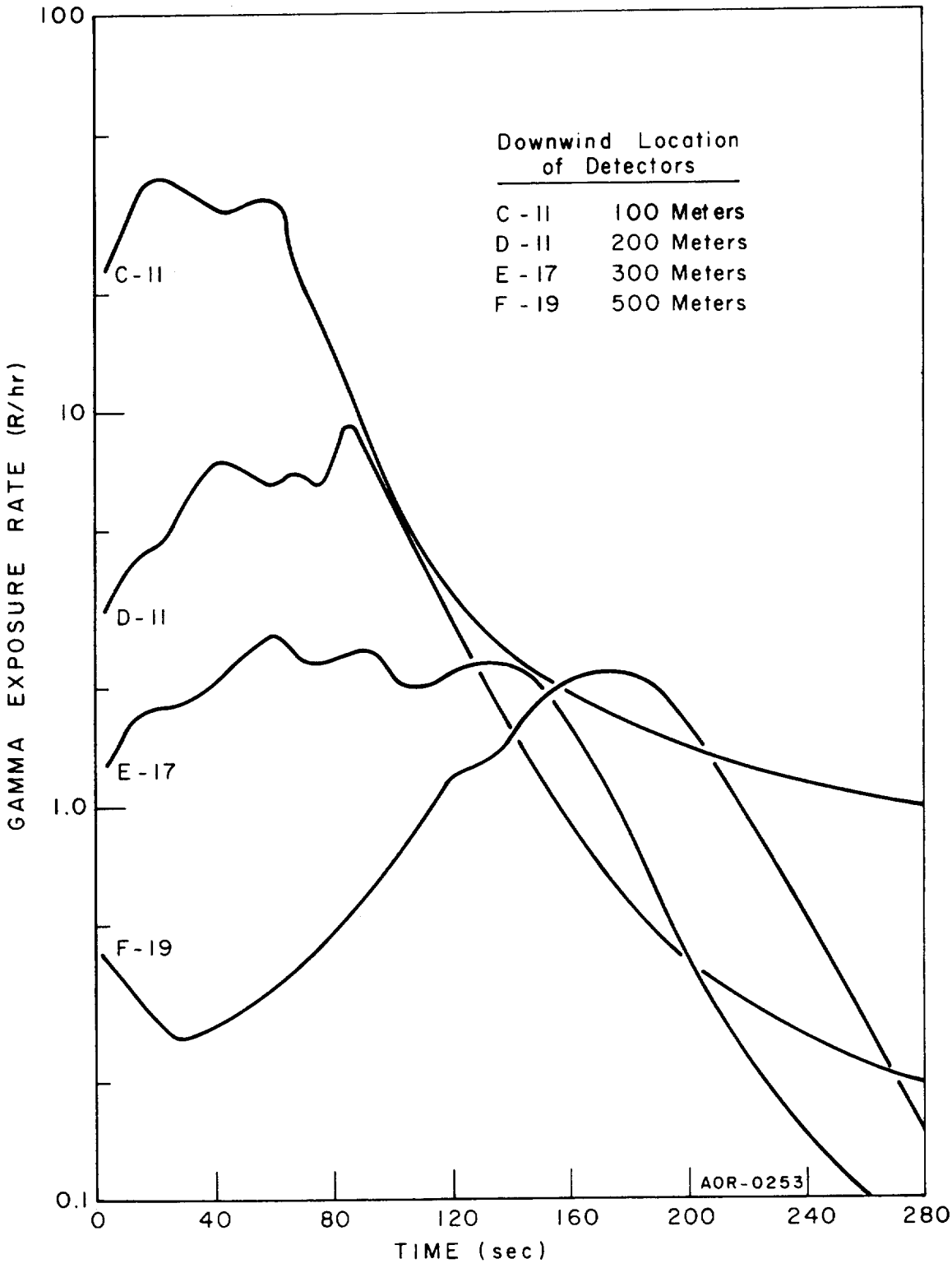

Fig. 17 Cloud dose rate measurements at downwind locations.

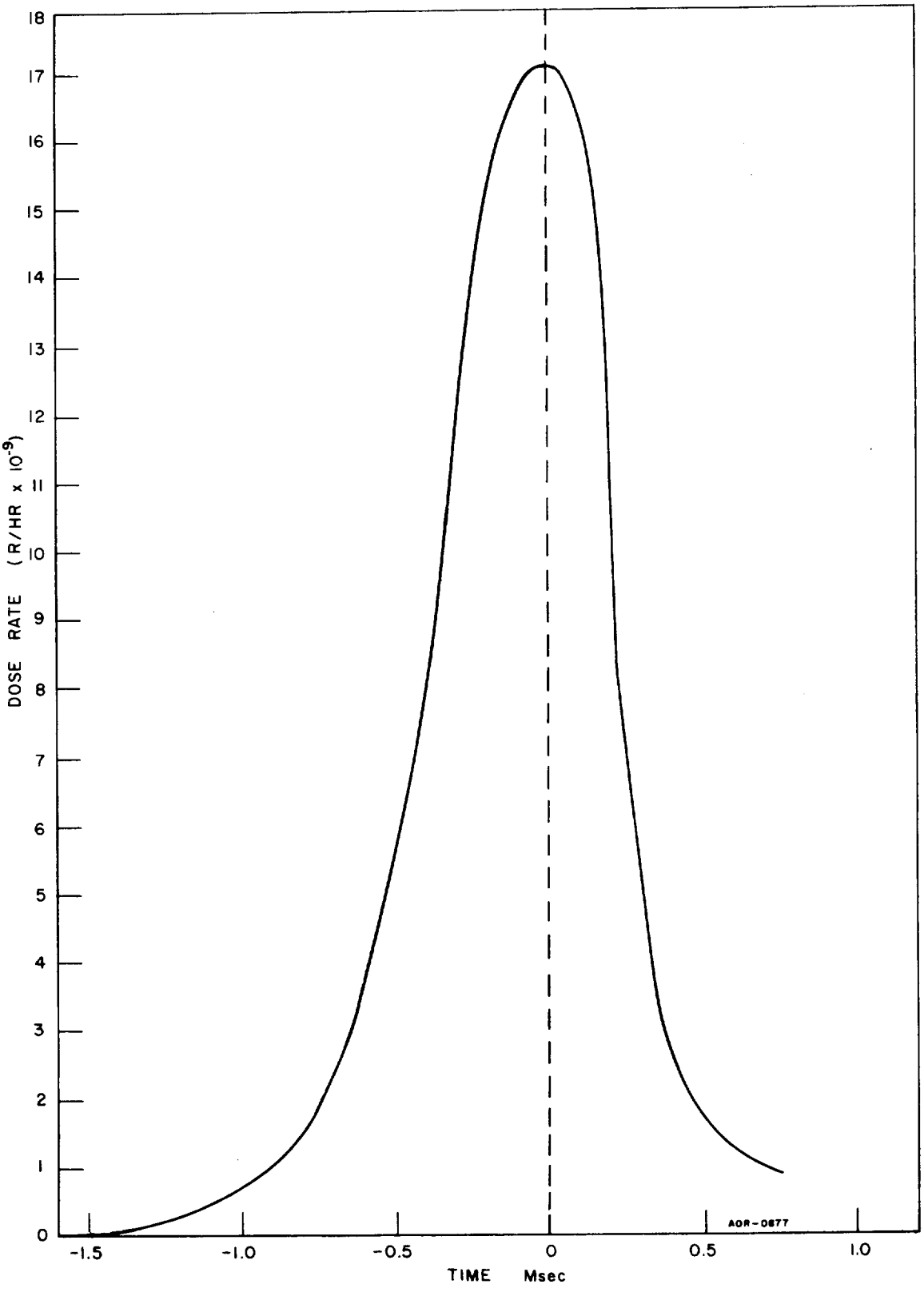

Fig. 18 Prompt gamma dose rate measured at 2.2 meters from the reactor.

2. TOTAL INTEGRATED DOSE MEASUREMENTS

The total integrated beta and gamma exposures resulting from the test were measured by film badge dosimeters, small ionization chambers, thermoluminescent dosimeters, and chemical dosimeters[8]. Neutron dose measurements were made with ORNL-Hurst type nuclear accident dosimeters and gold activation foils.

Many of the film dosimeters on the grid were shielded from the reactor transient radiation by topographical features of the test site. This shielding affected some of the exposures, as indicated by the grid film dosimeter readings which are shown in Figure 19 as a function of distance and direction. The greater readings along the 30 degree azimuth are a result of the radioactive cloud passing over this section.

The accumulated six-hour, unshielded, upwind, gamma exposure on a straight line from the reactor is given in Table IV.

The total prompt gamma dose was determined by integrating the prompt gamma dose rate measured by the short-response-time detector shown in Figure 18. Table V shows the total integrated doses obtained from two unshielded detectors near the reactor.

The neutron doses were monitored at four locations with Hurst-type nuclear accident dosimeters. These dosimeters were attached to a rope and pulley device so they could be quickly retrieved and counted following the test. Table VI summarizes the integrated neutron doses measured by these monitors.

Figure 20 shows the neutron and gamma doses along with the total integrated dose as a function of distance from the reactor. Measurements were made to determine the upper range of the total integrated exposure dose delivered by the destructive test including the prompt gamma-ray dose and the fission product decay dose at points near the reactor. To perform these dose measurements, a number of lithium fluoride (LiF) thermoluminescent dosimeters, calcium fluoride (CaF_2) thermoluminescent dosimeters, and chemical dosimeters were used in conjunction with film dosimeters at various locations around the reactor. Table VII lists the recorded doses as a function of distance, grid location, and dosimeter type.

The low exposure recorded by the film dosimeters at distances of less than 25 meters from the reactor is due to the exposure exceeding the 600 rem capability of the film. The discrepancies noted between various dosimetry methods are probably due to calibration factors, source geometry, neutron sensitivities, and dose-rate dependence problems which arose during the nuclear excursion. At positions where the exposure was relatively low, the disagreement between exposures recorded on film and lithium fluoride dosimeters is small. This discrepancy can be attributed to calibration factors.

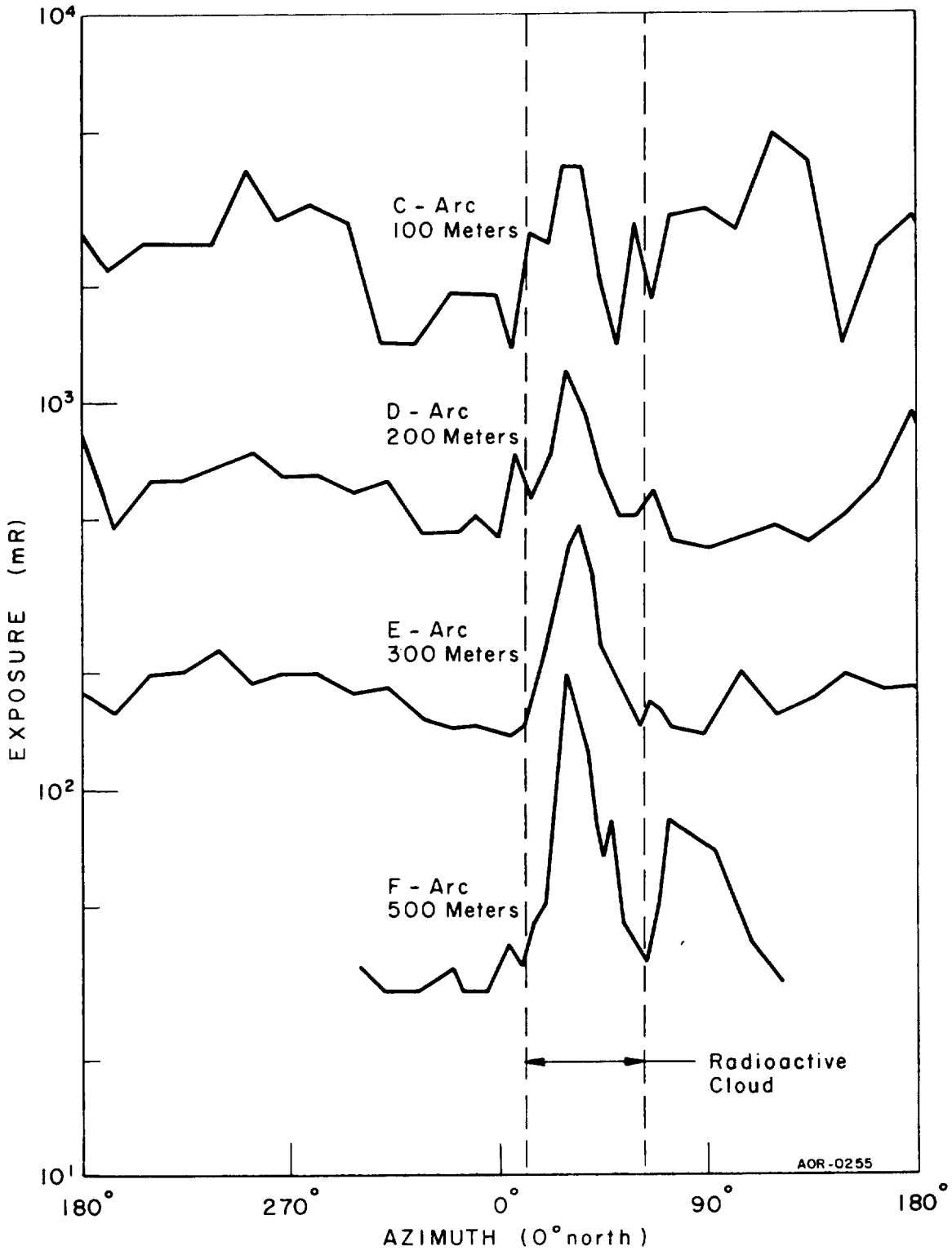

Fig. 19 Grid film -- dosimeter data.

TABLE IV

UPWIND FILM DOSIMETER READINGS

Distance (meters)	Grid Location	Dose (rem)
25	A-40	150
50	B-70	37
100	C-29	4
200	D-29	0.7
300	E-38	0.2

TABLE V

PROMPT INTEGRATED GAMMA DOSE

Detector Distance (meters)	Total Integrated Dose (rem)
2.2	3400
0.3	3800

TABLE VI

NEUTRON MEASUREMENTS

Distance (meters)	Dose (rem)
6.6	18,000
10.4	5,000
19	620

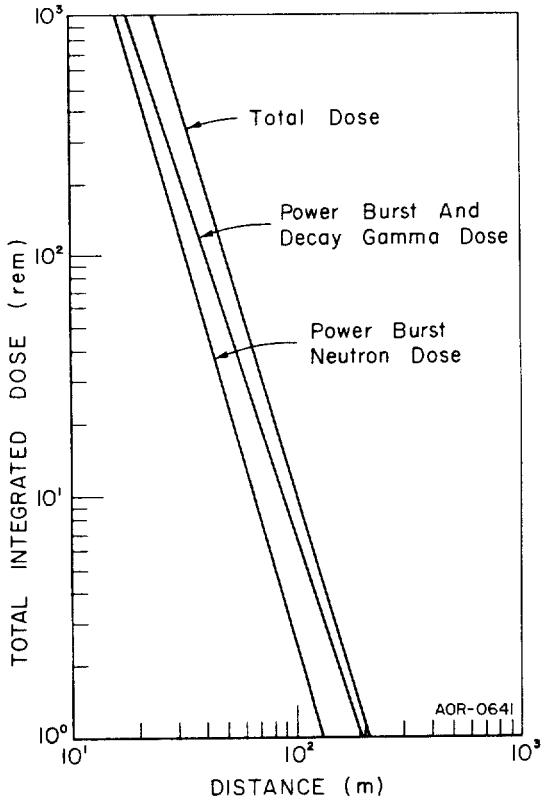

Fig. 20 Total integrated gamma and neutron doses.

TABLE VII

HIGH-RANGE DOSIMETER READINGS
(Dose in rem)

Distance (meters)	Grid Location	Film Dosimeter	Chemical Dosimeter	Thermoluminescent Dosimeter	
				CaF_2	LiF
2	2-6	600[a]	3600	4000	56,000
5.8	CL-1	600[a]	200-600	1400	29,000
8	CL-2	600[a]	---	---	4,900
10	10-24	---	710	510	---
25	A-40	150	---	---	370
50	B-70	37	---	---	53
100	C-29	0.74	---	---	0.9
300	E-38	0.19	---	---	---

[a] Exceeded the range of the dosimeter.

3. FUEL DISPERSAL

Wide spread dispersal of the fuel and beryllium reflector pieces was brought about by the high pressure generated within the fuel lattice. This pressure was generated by hydrogen being released from its bound state in the zirconium hydride fuel during the destructive excursion. Beryllium reflector pieces and fuel rod pieces were thrown to distances as great as 200 meters by the forces developed during the test. These forces also caused much of the fuel to fragmentize into small pieces. The immediate test area was extensively contaminated as a result of the test. The dispersion and concentration of fuel pieces and particles found in the test area are shown in Figure 21. A heavy concentration of material existed out to a radius of 10 meters. Between 10 and 50 meters the reactor fuel particles and pieces were somewhat less densely concentrated. Fuel particles between 50 and 100 meters from the reactor package were sparsley scattered and only a few relatively small pieces were located beyond 100 meters.

Figure 22 presents a before and after view of the top of the reactor and illustrates the complete disassembly of the core. Although the fuel elements and beryllium control drums are missing, very little damage was done to support fixtures and the superstructure. Reactor debris and fuel particles can be seen deposited on all horizontal surfaces.

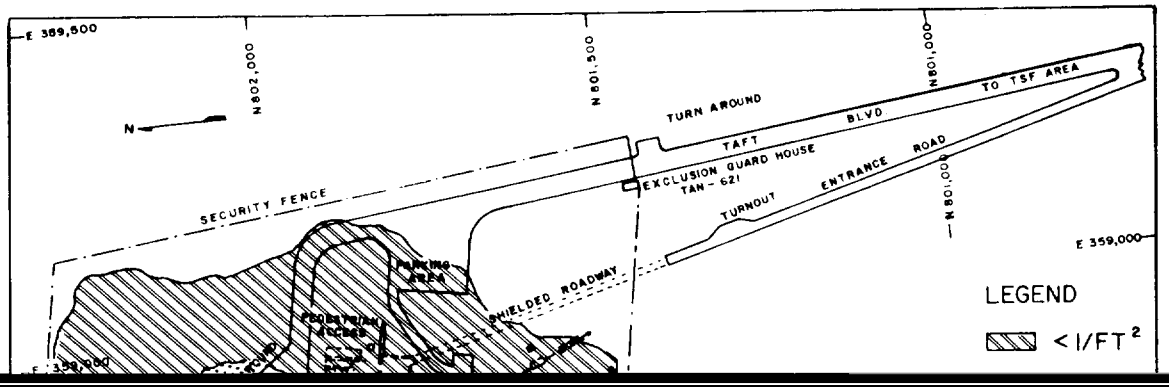
E 389,500
N 802,000
N 801,500
N 801,000
N
TURN AROUND
TAFT
BLVD
TO TSF AREA
SECURITY FENCE
EXCLUSION GUARD HOUSE
TAN - 621
TURNOUT
ENTRANCE
ROAD
N 800,500
E 359,000
PARKING AREA
SHIELDED ROADWAY
PEDESTRIAN ACCESS
LEGEND
< 1/FT²

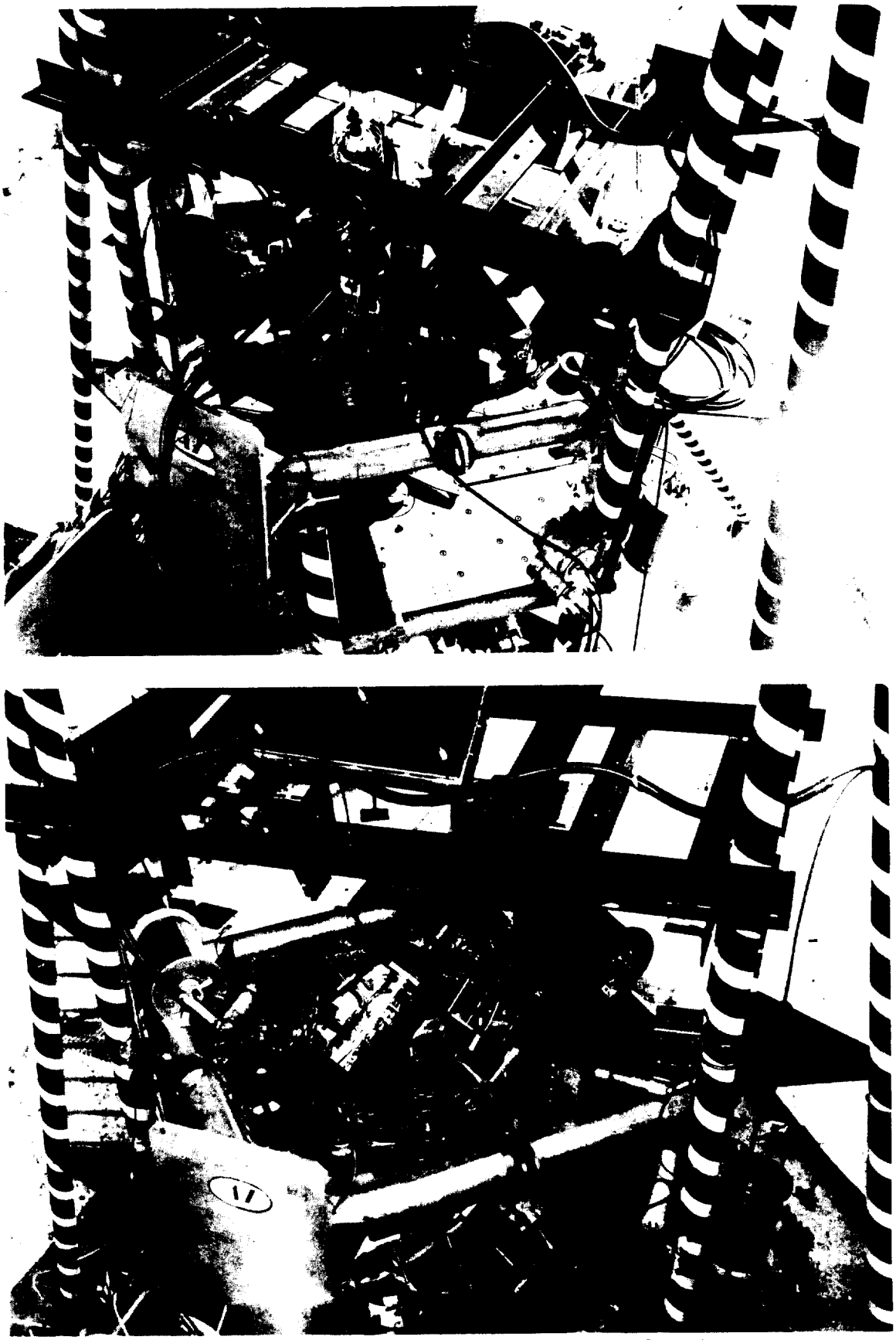

Fig. 22 Before and after view of the SNAPTRAN-2 reactor.

4. RELEASE OF FISSION PRODUCTS

Significant quantities of the following fission product nuclides were detected on the high-volume air sampler filters recovered from the radiological grid.

Sr-89, Sr-90, Sr-92

Y-91m, Y-92

Zr-Nb-95

Mo-Tc-99

I-131, I-132, I-133, I-134, I-135

Te-132

Xe-135

Cs-138

Ba-139, Ba-140

La-140, La-142

Ce-143

The measured amount of activity from each of the above nuclides was correlated with atmospheric diffusion data to estimate the total quantity of the nuclide or its precursor that was released from the reactor core. These quantities were compared with the total available to determine the release percentages shown in Table VIII. Mathematical models and calculational techniques used in these correlation analyses are presented in Section VIII.

TABLE VIII

PERCENT OF FISSION PRODUCTS RELEASED

Group	Released to the Atmosphere (percent)
Noble Gases	75
Iodines	70
Tellurium	45
Solids	4
Total Fission Product Inventory	21

The release of less than 100 percent of the noble gases from the fuel during the destructive excursion was not expected. It was generally assumed that the fuel material would be severely fragmented by the intense hydrogen pressure and that this would allow all of the noble gases to escape. The test experience indicates that while 100 percent of the noble gases were released from some of the fuel, a significant portion of the overall core maintained sufficient integrity to retain a considerable fraction of the noble gases. Viewed from another standpoint, the measure of the fraction of the noble gas released is probably an indication of the fraction of the fuel matrix that was completely fragmented. In the water immersion destructive test[11], the noble gas release was limited to approximately four percent, presumably because the cooling action of the water limited the fragmentation of the fuel matrix.

A second unexpected result of the test was the large fraction of the tellurium isotopes that were released. For most reactor safety analysis work, the tellurium isotopes are grouped with the "solid" portion of the fission product inventory. The 45 percent release of tellurium from this SNAPTRAN-2 test compared with the 4 percent release of solid fission products indicates that this assumption is not valid for reactor excursion accidents without a water environment. In the water immersion test, both the tellurium and "solid" fission products were completely retained by the fuel and water.

5. BERYLLIUM DATA

Because of the presence of beryllium in the reactor control system, it was necessary to monitor for this highly toxic, nonradioactive element in the event that some of it would become airborne as a result of the test. Special air samplers that could be recovered immediately after the test were assembled to sample the atmosphere over the reactor. The filters from these samplers were immediately recovered and analyzed for beryllium. Only background amounts of beryllium were detected. Several subsequent samples were taken at various intervals after the test, and they likewise showed that the beryllium from the reactor debris had not become airborne.

6. AUTORADIOGRAPHY OF FALLOUT PLATE AND AIR SAMPLER FILTERS

As an aid to determine the boundaries of the trajectory of the radioactive cloud, several fallout plates and all downwind air sample filters were exposed to X-ray film to obtain an autoradiograph of the collected radioactivity. This very sensitive technique demonstrated clearly whether or not a particular sampler had been exposed to the cloud. The fallout plate autoradiographs also indicated a density distribution of the particle fallout from the radioactive cloud. Figure 23 is a contact photograph of an autoradiograph of a fallout plate from grid position E-18, 300 meters downwind. The fallout material distribution is clearly visible. Figure 24 is a contact photograph of an autoradiograph of a typical air filter which had been exposed to the cloud at grid position G-20, 900 meters downwind.

One interesting phenomenon that was observed during the autoradiography work was the apparent size difference of particles that were collected near the reactor and those collected at greater distances downwind. Air samplers near the test site had a fine, even distribution of particles giving rise to an evenly exposed autoradiograph, as shown in Figure 25, from a sampler 200 meters from the test site. At 900 and 1500 meters downwind, the autoradiographs showed a nonuniform particle distribution. Figure 24 shows the typical autoradiograph from a filter 900 meters downwind. A comparison of these last two figures indicates that there may have been an agglomeration of the radioactive particles as they traversed the distance between the two samplers.

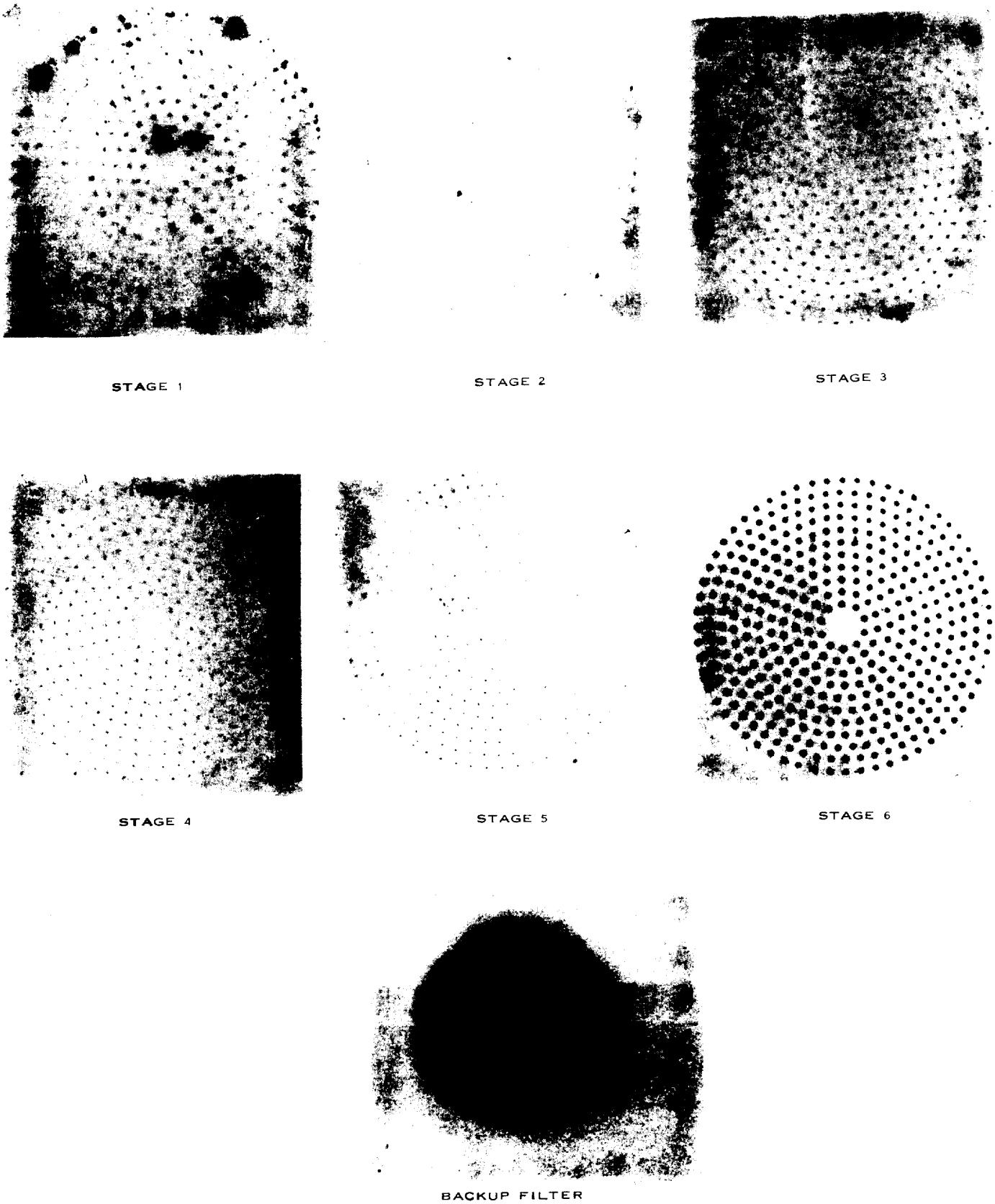

Fig. 23 Autoradiograph of stages of Anderson sampler.

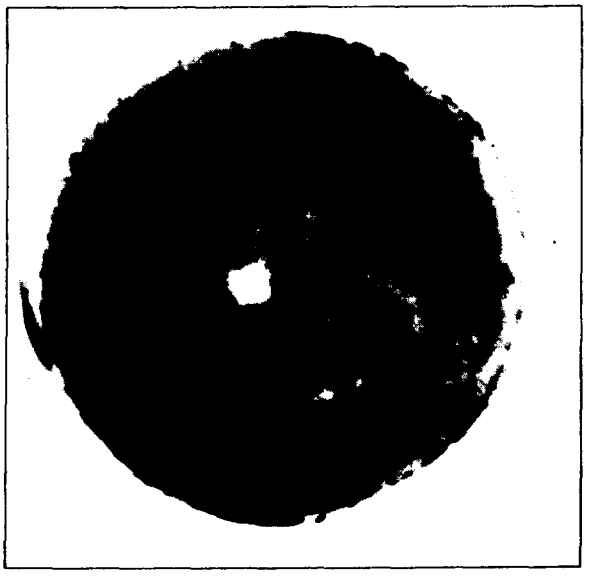

Fig. 24 Autoradiograph of air filter 900 meters downwind.

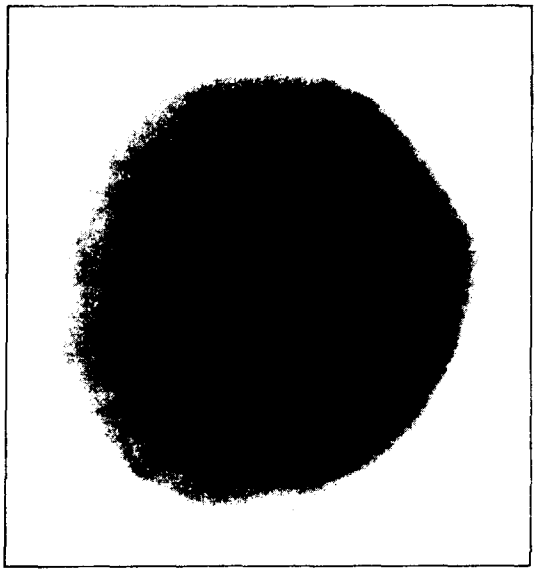

Fig. 25 Autoradiograph of air filter 200 meters downwind.

7. PARTICLE SIZE ANALYSIS

One of the objectives of the environmental sampling program was to determine the size of the particles associated with the airborne radioactivity released from the SNAPTRAN-2 test. Measurements were made on the inner arcs out to 200 meters using the Anderson impactor samplers. On the distant arcs, at 4000 and 8400 meters, particle sizing of the airborne radioactive material was accomplished using Unico cascade impactors. Additional particle sizing was accomplished by the visual counting of optical and electron microscrope photographs of dust collected on high-volume air sampler filters.

Data collected from the Anderson samplers indicated that the majority of the airborne radioactivity released from the test was associated with extremely small particles. Gross radiation counts of the various stages of the sampler showed that greater than 99 percent of the activity passed all six stages of the sampler and was collected on the backup particulate filter. The final stage of the Anderson sampler as operated during the test was capable of collecting particles down to one micron in size. Figure 26 shows autoradiographs taken of the sampling stages of an Anderson sampler and the backup filter. The backup filter from this sampler at station A-24 read 2.5 R/hr at 10 hours after the test.

At distances of 4000 and 8400 meters from the reactor, it was assumed that particles larger than 200 microns in diameter resulting from fragmentation of the reactor core would not remain airborne. Large radioactive particles collected at these distances would be expected to have formed from agglomeration of smaller particles or by sorption to larger atmospheric dust particles.

The results shown in Table IX were obtained from the analysis of a Unico cascade impactor which was located 4000 meters downwind. All stages were

Fig. 26 Autoradiograph of fallout plate 300 meters downwind.

TABLE IX

CASCADE IMPACTOR DATA (UNICO)

Stage Number	Activity (dis/min)	Activity on Each Stage (percent)	Stage MMD[a] (micron)	Less Than Stated Size[c] (percent)
1	6.6×10^2	14.3	---[b]	---
2	3.6×10^2	7.8	5.50	81.7
3	2.4×10^2	5.2	2.25	75.2
4	6.9×10^2	15.0	1.50	65.3
5(filter)	26.6×10^2	57.7	---[b]	---
Total	46.1×10^2	100.0	---	---

[a] Mass median diameters for each stage were calculated for silica having a density of approximately 2.6 g/cm^3. This calculation was based on the assumption that the activity was associated with atmospheric dust having essentially the same composition as the ground soil in the vicinity of the test.

[b] No meaningful calibration values can be assigned to stages No. 1 and No. 5 since the upper and lower size limits of the aerosol may be infinite.

[c] Percentages less than stated size were calculated by taking 1/2 the activity on the particular stage being examined plus all the activity passing that stage and then dividing the total activity measured.

counted for gross gamma activity, and this count was used to determine the percent of the material collected in each particle size range. This impactor had four stages backed by a membrane-type filter and was operated at a flow rate of 0.29 liter per second.

Because of the short duration of the cloud passage, conventional size selective samplers, such as the Unico and Anderson cascade impactors, could not obtain an adequate sample for particle size analysis by electron microscopy and visual counting. Instead, high-volume air samplers equipped with 20- x 25-cm filters were used on the 4000- and 8400-meter arcs. After these samples were collected, estimates of the particle size of the material collected were made by sizing and counting electron microscope photographs of the samples. The results, which include both radioactive and non-radioactive particles, are shown in Table X.

TABLE X

PARTICLE SIZE ANALYSIS OF AIR FILTERING

Downwind Distance (meters)	Count Median Diameter	Geometric Standard Deviation
4000	0.10μ	1.78
4000	0.135μ	2.07
4000	0.082μ	1.95
8400	0.21μ	1.57

The particle size measurments all indicated that the majority of the airborne radioactive material from the test was associated with particles of less than one micron in diameter with smaller amounts collected on larger particles. This was consistent with expectations, since most of the radioactive material in the cloud was initially atomic-sized daughter products of the noble gases. It was expected, however, that the atomic-sized daughter products would have been quite mobile and reactive and would have interacted with larger atmospheric particles by sorption. The most probable material for this interaction was the smoke in the visible cloud that was generated from burning fuel, plastic, paint, and grease during the excursion. Smoke has the required mass median diameter generally on the order of 0.5 micron[9]. However, this assumption does not rule out the possibility of some interaction with the normal condensation nuclei in the atmosphere which also have sufficiently small particle size to fit the observed measurements.

VIII. FISSION PRODUCT RELEASE ANALYSIS

Presented in this section is a brief summary of the considerations and analytical techniques used in analyzing the radiological grid data to obtain estimates of the fractions of the generated fission products that were released to the atmosphere as airborne material.

The general approach taken was to relate the amount of activity collected on the downwind grid samplers to the total quantity released by means of an atmospheric diffusion model based on statistical diffusion theory with an assumed Gaussian material distribution[10].

Using this approach, the integrated quantity of activity collected by a downwind air sampler which samples the entire cloud from an instantaneous puff release is represented by the equation

$$B = \left[F_o D_o + \sum_{i=1}^{n} F_i D_i \right] SE \left(\frac{X}{Q} \right) \qquad (1)$$

where

B = quantity of isotope under consideration collected by the sampler on the cloud center line (curies)

F_o = release fraction of the isotope under consideration produced by direct fission yield

D_o = calculated quantity of the isotope produced by direct fission yield available for release (curies)

F_i = fraction of the ith precursor released

D_i = calculated activity of the nth isotope from decay of the ith precursor (curies)

S = the sampling rate of the sampler (m^3/sec)

E = the collection efficiency of the sampler

$\frac{X}{Q}$ = the center line total integrated concentration from a puff source as obtained from the universal statistical diffusion equation assuming a Gaussian material distribution. That is,

$$\frac{X}{Q} = \frac{1}{\bar{u}\sigma_y\sigma_z} \exp\left[-1/2 \left(\frac{y^2}{\sigma_y^2} + \frac{h^2}{\sigma_z^2} \right) \right]$$

[redacted]

where

$\bar{u}$ = mean wind speed (m/sec)

σ_y = the standard deviation of the lateral dispersion (m)

σ_z = the standard deviation of the vertical dispersion (m)

h = the effective height of the release

Q = the source strength (curies)

X = the total integrated concentration at any distance of interest ($\frac{\text{curie-sec}}{m^3}$).

Equation (1) makes use of two assumptions that were not completely fulfilled by the SNAPTRAN-2 radioactive cloud. These were that the cloud originated as an instantaneous point source and that the cloud was not depleted by fallout between the release point and the receptor. It is felt that the effect of these two assumptions upon the release estimates was small. The effect of an initial cloud volume diminishes rapidly with distance, and the downwind measurements indicated that the point source approximation was valid. The effect of fallout depletion was investigated by estimating the total fallout on the grid from fallout plates and comparing this to the total activity released. Based on this comparison, fallout accounted for less than 0.5 percent of the corrected fission products, thereby introducing negligible error into the analysis.

It can be seen from Equation (1) that when the isotope under consideration, such as tellurium-132, is produced only by direct yield or from short-lived precursors (half-life < 1 sec), the summation quantity reduces to zero and Equation (1) can be solved directly for the release fraction. For cases in which the collected activity, such as iodine, comes from both direct yield and from the decay of radioactive precursors, Equation (1) was rewritten into Equation (2) which could be solved for the release fractions by the method of simultaneous equations.

$$\frac{B\left(\frac{X}{Q}\right)}{SE} = F_o D_o + F_1 D_1 + F_2 D_2 \qquad (2)$$

By comparing data from any two of the iodine-131, -132, -133, and -135 decay chains and by making the reasonable assumption that all of the iodine detected on the grid samplers came from either direct iodine yield or tellurium decay, release fractions for both tellurium and iodine were obtained.

Noble gas release values were obtained from Equation (1) using noble gases with sufficiently short half-lives such that all of the gas decayed into its particulate daughter before reaching the detector. The assumption was then made that all noble gases were released with the same fraction as those detected.

The above calculational techniques were then applied to the cloud center line samples from each of the arcs of the radiological grid beyond 300 meters. The results from the various arcs were averaged to determine a release fraction for the test. The data from the filters positioned closer than 500 meters from the reactor were not used in the initial release analysis because of the interference of small amounts of fuel dust and the uncertainty of the height of the cloud.

However, further attempts were made to use the data obtained from the samplers on the inner arcs to confirm the release fractions. As expected, the data from these samplers gave low release fractions because the initial release of the cloud was sufficiently high that it had not completely diffused to ground level. Therefore, the diffusion estimates for the inner arcs were made on the basis of the measured molybdenum-99 release fraction. The Mo-99

release fraction was first determined on sampling arcs sufficiently far from the test pad so as not to be affected by the initial cloud height. This fraction was then used to adjust the diffusion estimates on the close-in arcs to give the same Mo-99 release fraction. When this was done, reasonable agreement between the iodine, tellurium, and noble gas release was obtained for all arcs.

While these techniques did not remove all inconsistencies from the data collected from the grid, there was sufficient correlation between various sampling locations and independent measurements on different decay chains to give reasonable confidence in the release estimates obtained.

IX. DIRECT RADIATION ANALYSIS

An analysis was made to investigate the validity of simplified calculational techniques employed in theoretically predicting the direct radiation hazards associated with a nuclear reactor excursion such as that exhibited in the SNAPTRAN-2 experiment. Dose rates and total doses were calculated for comparison with experimental data. The calculations were based on the following general assumptions:

(1) The reactor excursion produced a total nuclear energy release of 54 MW-sec

(2) All fission products generated during the power burst were assumed to be distributed uniformly over a circular area 20 meters in diameter

(3) Shielding during the burst of power consisted of the steel vessel, beryllium reflector, self-shielding in the core, and air

(4) Attenuation following the power burst was due to air only.

Presented below are comparisons of calculated gamma dose rates, gamma doses, and neutron doses with corresponding experimental data. The techniques and equations used in the direct-radiation calculations are given at the end of this section.

1. DECAY GAMMA DOSE RATE

The points selected for comparison of analytical and experimental results were chosen in the W-SW direction from the reactor, which involved a minimal amount of shielding and was opposite to the direction of motion of the radioactive cloud. Shown in Figure 27 are the measured and calculated decay gamma dose rates versus time after the excursion at a point six meters from the reactor core and five feet above the ground. The experimental values for various decay times (see Table II) were obtained from a multipoint recording ionization chamber. A disk source 20 meters in diameter and centered on the ground beneath the detector position was assumed to obtain the calculated curve. The calculated results are in good agreement with the experimental values indicating that the assumed source geometry was a reasonable approximation.

The gamma dose rate versus time at a point three feet above the ground and 100 meters from the reactor (grid location C-29 in Figure 16) is shown in Figure 28. The measured curve was obtained with a constant-recording ionization-chamber apparatus. The assumed source geometry used to obtain the calculated curve was a line on the ground through the center of the test pad 20 meters long and perpendicular to the direction of the detector location from the reactor. The comparison of curves in Figure 28 indicates that the assumed source geometry yields somewhat conservative results.

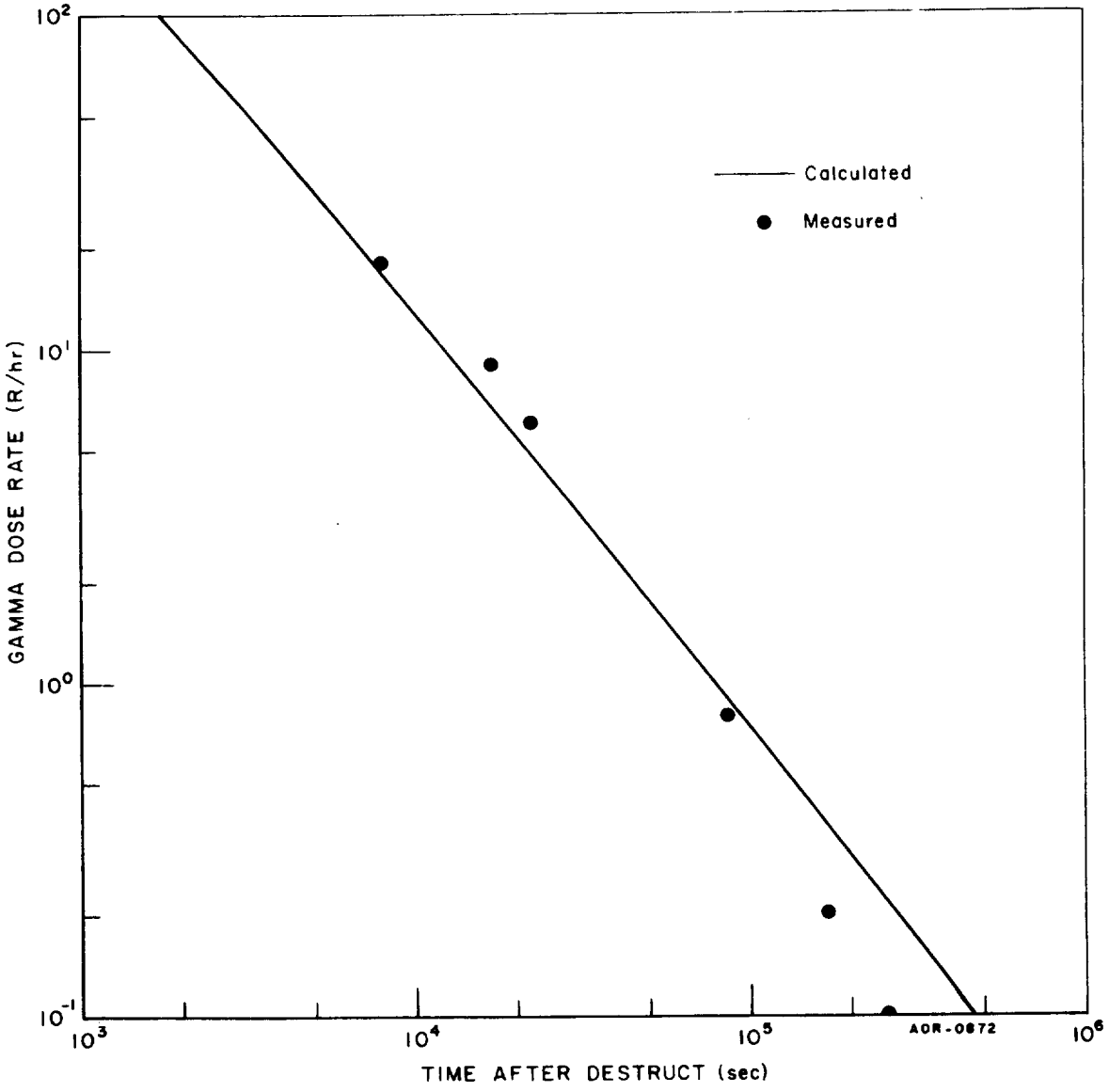

Fig. 27 Gamma dose rate 6 meters from reactor center.

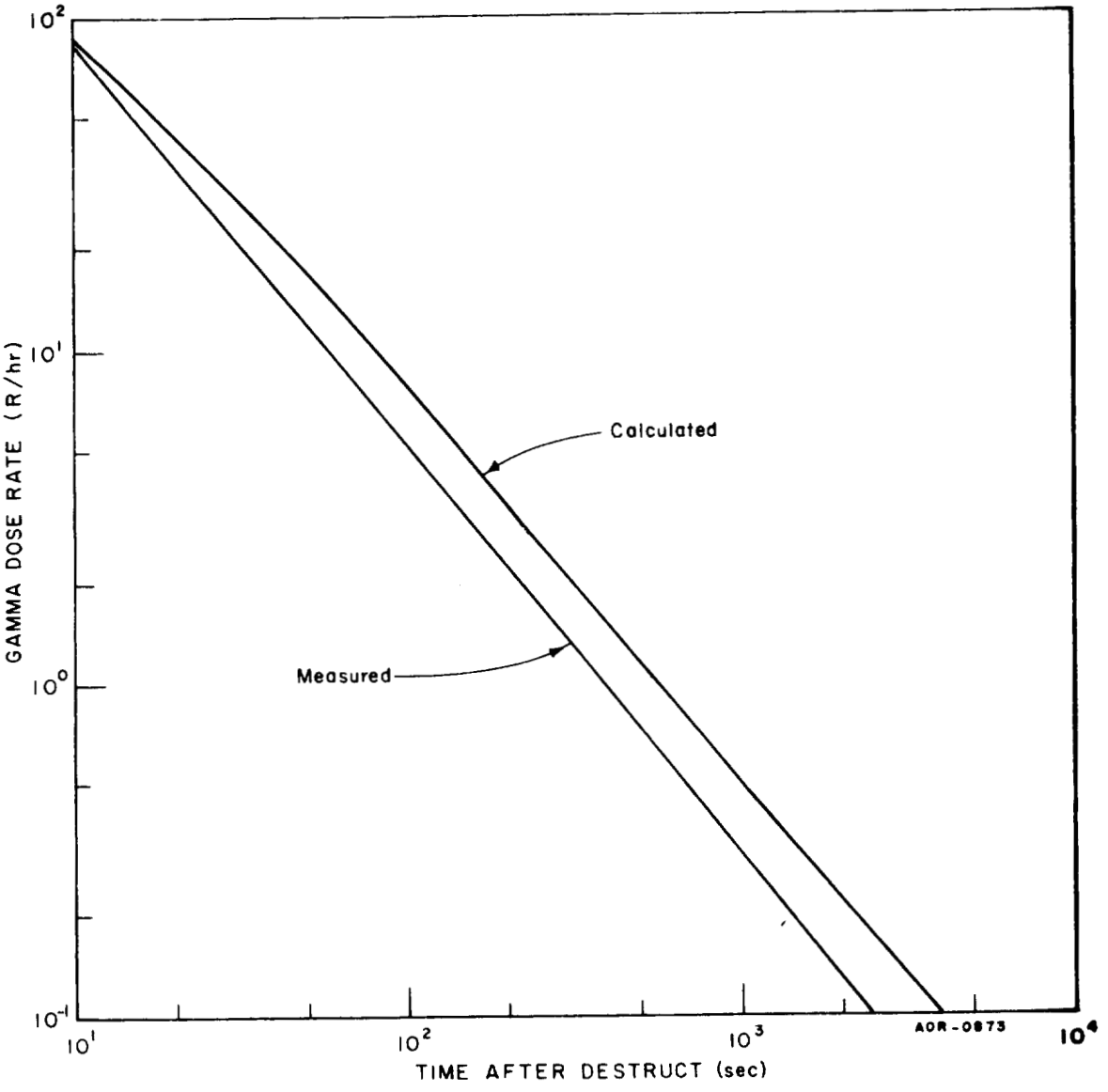

Fig. 28 Gamma dose rate at 100 meters from reactor center.

2. TOTAL GAMMA DOSE

The total gamma dose from direct radiation is due to prompt fission gammas accumulated during the burst of power and to fission product decay gammas accumulated after the burst. The calculated gamma doses (prompt, decay, and total) versus distance from the reactor are shown in Figure 29. Comparison was made with the total gamma doses measured by film badge dosimeters located three feet above the ground on the 25-, 50-, 100-, 200-, and 300-meter arcs. The corresponding grid locations in Table IV are A-40, B-70, C-29, D-29, and E-38, respectively.

A point source geometry was used to calculate the prompt gamma dose. The decay gamma dose curve was obtained by calculating the decay dose rate at various distances as a function of time and integrating the results for each distance over the film badge exposure time which was six hours. The assumed source geometry for calculating the decay dose rates was a line identical to that used to obtain the calculated curve in Figure 28.

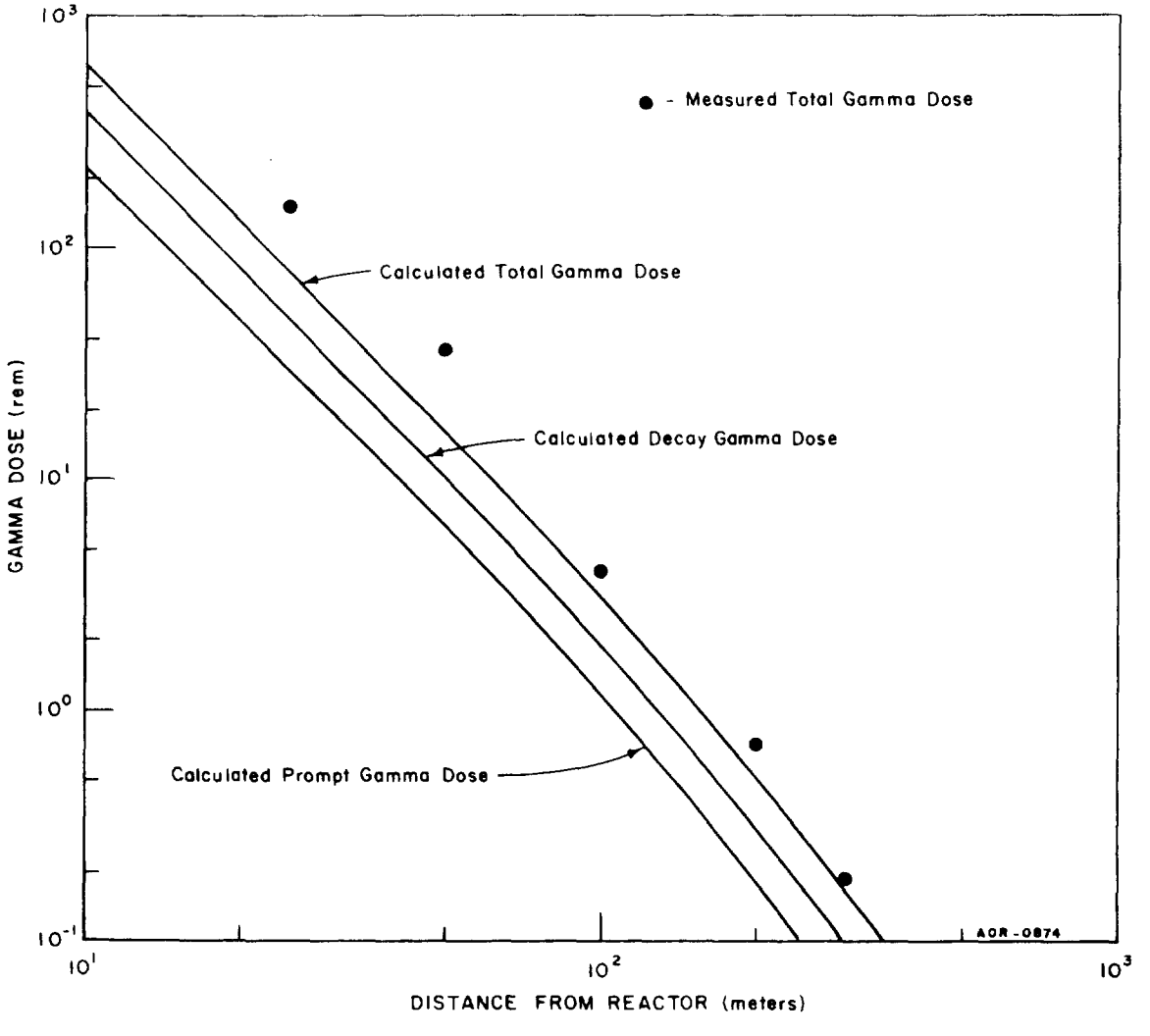

Fig. 29 Total gamma dose versus distance.

As shown in Figure 29, the measured doses at 25 and 50 meters are approximately a factor of two higher than the calculated values. This is due to the difference between the line source on the reactor pad assumed for calculations and the actual source distribution which resulted in the experiment. As may be seen in Figure 21, the 25- and 50-meter locations in the W-SW direction are in areas which contained averages of 50 and 10 fuel particles per square foot, respectively. Thus, a significant portion of the source activity was in the immediate area of the film badges at these locations.

3. NEUTRON DOSE

The calculated fission neutron dose versus distance from the reactor is shown in Figure 30. Comparison is made with the measured doses at 6.6, 10.4, and 19 meters from the reactor. A point source geometry was used to obtain the calculated curve. As shown in the figure, the measured doses decrease with distance more rapidly than the calculated values although there is reasonable agreement in magnitude.

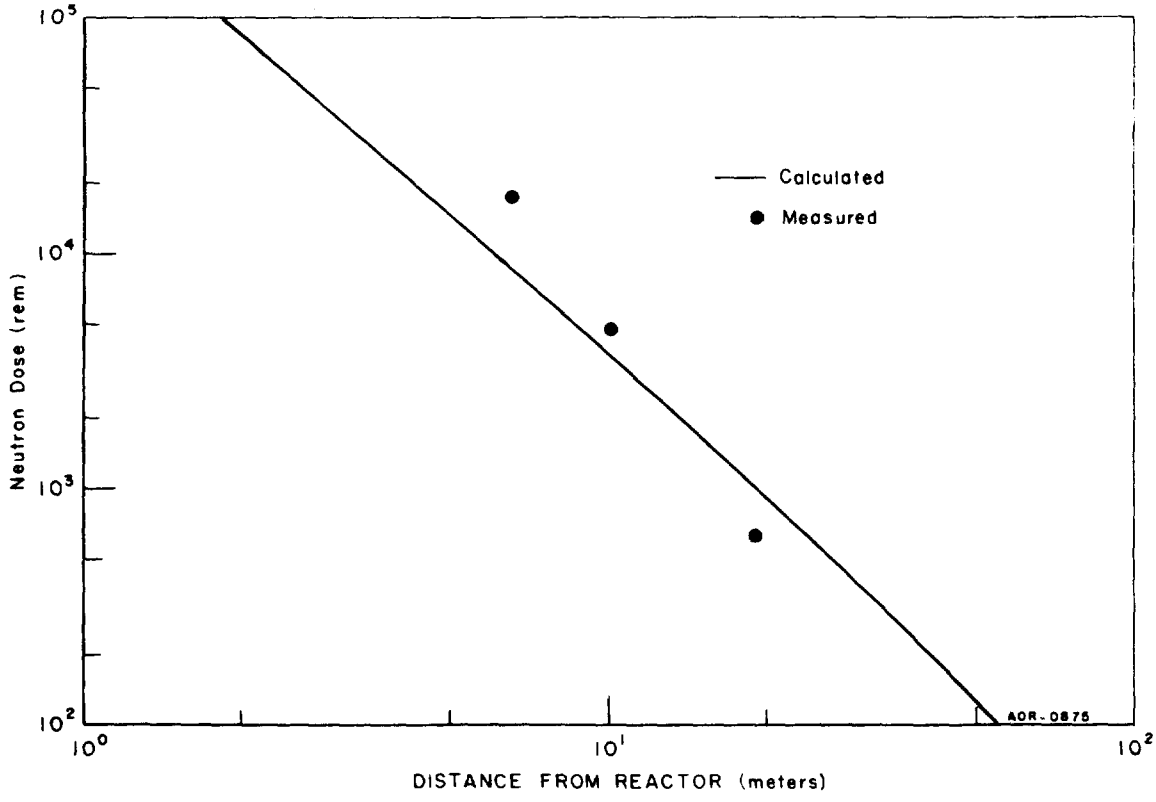

Fig. 30 Neutron dose versus distance.

4. DISCUSSION AND CONCLUSION

The accuracy of the foregoing calculated results is somewhat limited by differences between the simplified assumptions regarding fission product source geometries and the more complex actual configurations. As previously noted, the cylindrical geometry of the reactor prior to disassembly was approximated by a point source for calculations of the doses from prompt gamma rays and neutrons during the power burst. For calculations of the decay gamma dose rate and integrated gamma dose following the destructive excursion, the source was assumed to consist of the entire fission product inventory uniformly distributed over a circular area as noted in the general assumptions at the beginning of this section. In the actual experiment, some of the fission products (approximately 20 percent) were carried downwind in the radioactive cloud. Furthermore, as shown in Figure 21, the fission products remaining on the ground in the vicinity of the test facility were distributed in a complex, nonuniform pattern which varied considerably from the assumed circular distribution. In addition to the geometrical simplifications, the prompt gamma spectrum and decay gamma spectrum were each assumed to be represented by only three effective energy groups and the prompt neutron spectrum by only one group. The assumed energy group values are presented below under Analytical Techniques. All of these factors contribute to some uncertainty in the calculations.

As stated in the introduction to this section, the objective of this analysis was to investigate the validity of simplified calculational techniques. In spite of the simplifications and approximations discussed above, it may be seen in the comparisons of data that the calculated results deviate from the experimental values by no more than a factor of two.

In view of the uncertainties associated with predicting the release, transport, and distribution of fission products following a reactor accident, it is concluded that the results of this analysis agree sufficiently with the SNAPTRAN-2 experimental data to justify the use of similar techniques in predicting the direct radiation hazards associated with destructive excursions involving other unshielded reactor systems.

5. ANALYTICAL TECHNIQUES

The calculated gamma dose rate in Figure 27 was obtained using the following equation for a disk source with no shielding[11]:

$$\Phi = \frac{S_A}{2} \ln \sec \theta$$

where

Φ = gamma flux at detector position (γ's/cm^{2}sec) of energy, E_γ, at decay time, t

S_A = plane source strength (γ's/cm^{2}sec) of energy, E_γ, at decay time,

$$t = \frac{3.1 \times 10^{10} P t_o f(t, E_\gamma) E_T(t)}{A E_\gamma}$$

Pt_o = integrated nuclear energy release (5.4×10^7 W-sec)

$f(t,E_\gamma)$ = fraction of $E_T(t)$ with energy, E_γ

$E_T(t)$ = total gamma energy release rate (MeV/fiss-sec)

A = area of disk (cm^2)

θ = $\tan^{-1}$ (R/a)

R = radius of disk (10^3 cm)

a = distance from detector position to disk (152 cm).

The spectrum of gamma energy was assumed to be represented by three effective energies (0.9, 1.8, and 2.6 MeV). Values of $f(t,E_\gamma)$ and $E_T(t)$ were obtained from spectral curves in Reference 12. Factors for converting flux to dose rate were obtained from Reference 11.

The dose rate versus time in Figure 28 was calculated based on the following equation for a line source[11]:

$$\Phi = \frac{S_L}{2\pi a} F(\theta, b_1)$$

where

S_L = line source strength (γ's/cm sec) of energy, E_γ, at decay time, $t = \frac{3.1 \times 10^{10} Pt_o f(t,E_\gamma)\ E_T(t)}{L E_\gamma}$

L = length of line (2×10^3 cm)

a = distance from detector position to line (10^4 cm)

$$F(\theta,b_1) = \int_0^\theta e^{-b_1 \sec \theta} d\theta$$

θ = $\tan^{-1}$ (L/2a)

$b_1 = \mu a$

μ = linear absorption coefficient for air (cm^{-1}).

The other quantities are as previously defined. Values of $E_T(t)$ for decay times less than 300 seconds were obtained from Reference 13. Those for longer decay times were taken from Reference 12.

The calculated decay gamma dose versus distance (Figure 29) was obtained by numerically integrating the decay dose rate curves for several distances as computed with a line source similar to that above.

A point source geometry was used to calculate the prompt gamma dose versus distance (Figure 29) based on the following equation[11]:

$$\Phi = \frac{S_o}{4\pi a^2} e^{-b_2}$$

where

Φ = integrated prompt gamma flux at detector position (γ's/cm^2) of energy, E_γ

S_o = point source strength (γ's/sec) of energy, $E_\gamma = \frac{3.1 \times 10^{10} Pt_o Y(E_\gamma)}{E_\gamma}$

$Y(E_\gamma)$ = 2.89, 2.26, and 2.04 MeV/fiss at E_γ = 0.8, 2.0, 4.0 MeV, respectively[14]

$b_2 = b_1 + \mu_s z$

$b_1 = \sum \mu_i t_i$

μ_i = linear absorption coefficient for the ith shield (cm^{-1})

t_i = thickness of the ith shield (cm)

μ_s = energy absorption coefficient for the core material (cm^{-1})

z = effective self-attenuation distance of the core if a cylindrical source were assumed

a = distance from reactor to detector position (cm).

Factors for converting the integrated prompt gamma flux to dose were taken from Reference 11. The calculated prompt gamma dose results thus obtained were increased by a factor of two to account for the contribution from the decay of very short-lived fission products.

The prompt neutron dose versus distance (Figure 30) was calculated based on the point source equation given above with

Φ = integrated prompt neutron flux at detector position (neutrons/cm^2) of energy equal to 1.0 MeV

$S_o = 3.1 \times 10^{10}\ Pt_o N$

N = average number of neutrons/fission = 2.46

μ_i = effective neutron removal cross section for the ith shield (cm^{-1})

μ_s = effective neutron removal cross section for the core material (cm^{-1}).

The other quantities are as previously defined. Numerical values for all absorption coefficients as a function of energy were obtained from Reference 11.

X. CONCLUSIONS

The fission product release from the SNAPTRAN-2 destructive test performed in open air was considerably higher than that released from the SNAPTRAN-3 underwater destructive test[1]. In the SNAPTRAN-3 test, only 4 percent of the noble gases, which constituted less than one percent of the total fission product inventory, was released. In the SNAPTRAN-2 test, 75 percent of the noble gases, 70 percent of the halogens, 45 percent of the tellurium, and 4 percent of the remaining solids were released. It is postulated that this difference in release fractions of fission products was due to the quenching action of the water on the fuel in the underwater test. This conclusion is based on the fact that only a small amount of noble gases was released to the atmosphere from the underwater test. Since noble gases do not readily react with water or other materials, it appears that the noble gas fission products were trapped in the fuel lattice of the quickly cooled fuel.

The fission product release results also indicate that it is virtually impossible to get 100 percent release of fission products from a reactor accident. The release of only 75 percent of the noble gases from the SNAPTRAN-2 destructive tests indicates that when a complete reactor core is involved, even in an extreme reactivity accident, a portion of the core will retain sufficient integrity to trap and hold a significant quantity of the fission products. Conversely, the 25 percent retention of noble gas fission products is probably an indication of the fraction of the fuel that retained sufficient integrity to holdup the noble gases.

The SNAPTRAN-2 test data indicate that the tellurium fission products demonstrated considerable volatility under the condition of the SNAPTRAN-2 test. The measured 45 percent release fraction was considerably higher than the general "solids" fraction of 4 percent. Since tellurium decays to the "biologically significant" iodines, this increased release of tellurium should be factored into radiological hazards analyses for safety analysis reviews of certain classes of reactor accidents. These accidents would be reactivity accidents with low inventory cores that are not contained in a water environment. For a core with a high inventory, the iodine contribution from tellurium decay will be negligible compared to the existing iodine inventories. For a water-environment core, the tellurium would be removed by the water.

Another important conclusion regarding the safety aspects of the SNAP 10A/2 reactors that can be drawn from the SNAPTRAN-2 test is that the beryllium from the drums and core reflector does not produce a health hazard by shattering into airborne dust particles. Numerous samples taken during and subsequent to the SNAPTRAN-2 test showed no detectable beryllium.

The direct radiation analysis demonstrated that simplified calculational techniques and assumptions could be used to predict the direct radiation levels associated with a SNAP 10A/2 destructive excursion. Based on the reasonable agreement between the calculated results and the SNAPTRAN-2 experimental data, it is concluded that similar techniques are applicable in predicting the direct radiation hazards associated with destructive excursions involving other unshielded reactor systems.

The SNAPTRAN-2 test confirmed the results of the SNAPTRAN-3 test that a reactivity accident with a "virgin fueled" SNAP 10A/2 reactor does not pose

any undue hazard to the general public. The total integrated radiation exposure dose at the NRTS site boundary (10^4 meters) was less than 10 mR for both tests. Likewise, the spread of contamination was limited to a radius of 200 meters from the reactor following both tests.

XI. REFERENCES

1. O. L. Cordes et al, Radiological Aspects of SNAPTRAN 2/10A-3 Destructive Test, IDO-17038 (January 1965).

2. Gelman Instrument Company, 600 South Wagner Road, Ann Arbor, Michigan, 48106.

3. Mine Safety Appliances Company, 201 North Braddock Avenue, Pittsburgh, Pennsylvania, 15208.

4. Union Industrial Equipment Corporation, 150 Cove Street, Fall River, Massachusetts, 02720.

5. Research Report No. 108, Dugway Proving Grounds.

6. G. S. Hurst and R. H. Ritchie (eds.), Radiation Accidents: Dosimetric Aspects of Neutron and Gamma-Ray Exposures, ORNL-2748 (Pt. A) (November 1959) p 24.

7. W. E. Kessler et al, SNAPTRAN-2 Destructive Test Results, IDO-17194 (January 1967).

8. Edgerton, Germeshausen, and Grier, Incorporated, Santa Barbara Laboratories Division, Box 98, Goleta, California, 93017.

9. H. L. Green and W. R. Lane, Particulate Clouds: Dusts, Smokes, and Mists; their Physics and Physical Chemistry and Industrial and Environmental Aspects, London: E. and F. N. Spon, 1957, p 352.

10. G. R. Yanskey, E. H. Markee, Jr., and A. P. Richter, Climatography of the National Reactor Testing Station, IDO-12048 (January 1966).

11. T. Rockwell, III (ed.), Reactor Shielding Design Manual, TID-7004 (March 1956).

12. J. F. Perkins and R. W. King, "Energy Release from the Decay of Fission Products", Nucl. Sci. Eng., 3 (June 1958) pp 726-746.

13. J. K. Warkentin, Gamma Energy Release from Fission Product Decay Following a Short Reactor Transient, IDO-17161 (April 1966).

14. K. Shure and G. L. Strobel, "Effective Neutron Capture Gamma Ray Spectra", Bettis Technical Review, WAPD-BT-22 (March 1961) pp 19-30.